The Role of Negative Carbon Dioxide Emissions in Climate System Reversibility

by

Katarzyna Barbara Tokarska

B.Sc. (Physics), Simon Fraser University, 2012

Thesis Submitted in Partial Fulfillment of the
Requirements for the Degree of
Master of Science

in the
Department of Geography
Faculty of Environment

SIMON FRASER UNIVERSITY

Summer 2014

Approval

Name: **Katarzyna Barbara Tokarska**

Degree: **Master of Science (Geography)**

Title: ***The Role of Negative Carbon Dioxide Emissions in Climate System Reversibility***

Examining Committee: **Chair:** Anders Knudby
Assistant Professor

Kirsten Zickfeld
Senior Supervisor
Assistant Professor

Gwenn Flowers
Supervisor
Associate Professor
Department of Earth Sciences

Ken Denman
External Examiner
Professor
School of Earth and Ocean Sciences
University of Victoria

Date Defended: June 27, 2014

Partial Copyright Licence

Abstract

The current trend of rising atmospheric CO_2 concentrations is likely to lead to harmful changes in Earth's climate system. This research explores the role of artificial atmospheric CO_2 removal (referred to as negative emissions) in reversing human-induced climate change. We designed a range of plausible CO_2 emission scenarios, which follow a gradual transition from a fossil fuel driven economy to a zero-emission energy system, followed by a period of negative emissions. The climate system components' responses are computed using the University of Victoria Earth System Climate Model of intermediate complexity.

The results suggest that while it is possible to restore global mean temperature to a lower level after overshoot (i.e. 2°C above pre-industrial), sea level rise is not reversible for several centuries, despite implementation of large amounts of negative emissions. Outgassing of CO_2 from terrestrial and marine carbon sinks offsets the artificial removal of atmospheric CO_2, thereby reducing its effectiveness.

Keywords: Negative emissions; Artificial Carbon Dioxide Removal; Terrestrial and Ocean Carbon Storage; Carbon Sinks Outgassing; Reversibility; Sea Level Rise

To my loving parents, Agata and Ryszard,
brother Tomek, and all those who supported me
during my research and graduate work.

Acknowledgements

I would like to thank Dr. Kirsten Zickfeld, my senior supervisor, for her guidance and encouragement, as well as helping me to understand the processes governing the Earth's climate system and showing me how to get started with running the UVic ESCM model.

In addition, I would like to thank Dr. Gwenn Flowers for her insights and helpful suggestions regarding the thesis structure and writing style.

Special thanks to Dr. Jaccard for providing me preliminary constructive feedback about the negative CO_2 emission technologies, fuelling my interest in that area, and challenging me to think outside the box.

Also, I would like to recognize Dana Ehlert and Tyler Herrington for helping me to get started with running the UVic ESCM model and providing valuable comments during the analysis of results.

This research was funded through a National Science Engineering and Research Council of Canada (NSERC) Discovery Grant awarded to Dr. Zickfeld.

Table of Contents

List of Tables

List of Figures

List of Acronyms

BioCCS	Biomass Energy with Carbon Capture and Storage
CCE	Constant Cumulative Emissions (Pathway Name)
CCS	Carbon Capture and Storage
CCR	Climate Carbon Response
DIC	Dissolved Inorganic Carbon
EBM	Energy Balance Model
EMIC	Earth System Model of Intermediate Complexity
ESM	Earth System Model
GCM	General Circulation Model
GtC	Giga-tonnes of Carbon
IPCC	Intergovernmental Panel on Climate Change
MOSES	Met Office Surface Exchange Scheme
NPP	Net Primary Productivity
RCP	Representative Concentration Pathway
TCRE	Transient climate response to cumulative emissions
TRIFFID	Top-down Representation of Interactive Foliage and Flora including Dynamics
UNFCC	United Nations Framework Convention on Climate Change
UVic ESM	University of Victoria Earth System Model
VCE	Variable Cumulative Emissions (Pathway Name)

Glossary

Cumulative Emissions	Annual CO_2 emission rate integrated over a specified period of time, equivalent to the total amount of CO_2 emitted, usually expressed in giga tonnes of carbon (GtC)
Negative Emissions	Artificial removal of the atmospheric CO_2 through one of the net-negative emission technologies available (e.g. direct air capture or biomass combustion with carbon capture and storage). As a result, there is a net decline in atmospheric CO_2 levels
Thermosteric Sea Level Rise	Rise in sea level due to the thermal expansion of the ocean

Chapter 1. Introduction

1.1. Problem Statement

Our continuously growing global economy emits carbon dioxide (CO_2) and other greenhouse gases to the atmosphere at a rapid rate (estimated at 9.67 GtC per year in 2013; Le Quéré et al., 2013). Natural carbon sinks in the ocean and terrestrial biosphere absorb approximately half of the emitted CO_2 (Le Quéré al., 2009). However, the rate of anthropogenic CO_2 emissions exceeds the rate of natural carbon dioxide uptake, leading to an increase in the atmospheric CO_2, which alters the Earth's climate with potentially harmful consequences for natural and human systems. Elevated atmospheric CO_2 levels also impact the hydrologic cycle, leading to an increase in global mean precipitation (Allen et al., 2002; Solomon et al., 2009) and changes in its regional variation, with a greater contrast between arid and wet regions (IPCC, 2013). Furthermore, intensification in severity and frequency of extreme weather events may follow, together with thinning of the sea ice cover, increased ice sheet ablation and a continual rise of the sea level (IPCC, 2013). The United Nations Framework Convention on Climate Change (UNFCCC) calls for stabilization of atmospheric greenhouse gas concentrations to avoid "dangerous anthropogenic interference with the climate system" (UNFCCC, Article 2, 1992).

In December 2009, at the United Nations Climate Change Conference in Copenhagen, many countries agreed to the ambitious goal of stabilizing the global mean temperature at 2˚C above the pre-industrial level (UNFCCC Conference of the Parties, 2009). To achieve this global temperature target, developed countries would need to reduce their emissions by 20% above their 1990s levels by 2020 and by 80%-95% by 2050 (Macintosh, 2010).

Reaching the CO_2 emission reduction levels needed to meet the 2°C target is difficult on a global scale, given that between 2000 and 2008, the global fossil fuel emissions increased by 29% (Le Quéré et al., 2009). This increasing trend in CO_2 emissions is likely to continue for coming decades, thereby exceeding the 2°C target, unless binding agreements are implemented on a global scale (Kypreos, 2012). A continued rise in atmospheric CO_2 increases the risk of exceeding dangerous thresholds in the climate system (e.g. ecosystem collapse, irreversible mass loss of ice sheets). Therefore, the question arises of whether it may be possible to revert to lower levels of climate change once dangerous thresholds are reached.

The current literature shows that in the case of complete cessation of CO_2 emissions, climate change is irreversible on centennial timescales (Matthews & Caldeira, 2008) or even up to 1000 years after the cessation of emissions (Eby et al., 2009; Gillett et al., 2011; Solomon et al., 2009). Irreversibility implies that the system does not return to its initial state (pre-industrial or 20th century) on human timescales after elimination of CO_2 emissions. While the system may be restored to its initial state on geological timescales, this is beyond the time frame relevant for human civilization (Boucher et al., 2012). However, with negative emissions that artificially remove CO_2 from the atmosphere, it may be possible to restore the climate system components to their previous states on human timescales.

1.2. Research Questions

The purpose of this research is to explore the reversibility of climate system components under scenarios that entail artificial removal of the CO_2 from the atmosphere. In particular, this research addresses the following research questions:

- Is it physically possible to exceed a specific level of climate change and return to it on centennial timescales if CO_2 is artificially removed from the atmosphere?
- How effective are negative emissions in decreasing the concentration of atmospheric CO_2, and hence, reversing the response of various climate system components?
- How do the natural carbon sinks (terrestrial and marine) react to artificial removal of atmospheric CO_2?

To address these questions, a range of CO_2 emission pathways are designed, which follow a smooth transition from a fossil-fuel based economy to a zero-emission energy system over the next 100 years and include implementation of negative emissions. The response of climate system components to these emission pathways is computed using the University of Victoria Earth System Climate Model of intermediate complexity (UVic ESCM).

1.3. Structure of the Thesis

Chapter 2 of the thesis provides an overview of the current literature about the climate system response to different CO_2 emission pathways and an introduction to net-negative emission technologies. Chapter 3 provides a description of methodology used to address the research questions, while Chapter 4 presents the results. Chapter 5 discusses the model uncertainties and risks related to the implementation of net-negative emission technologies, followed by Chapter 6, which provides a conclusion and highlights the novelty of the results from this study.

Chapter 2. Background

2.1. Atmospheric Lifetime of CO_2 and Thermal Inertia

The longevity of CO_2 in the atmosphere and delayed warming of the climate system (often referred to as thermal inertia) are important concepts in understanding the climate system response to anthropogenic CO_2.

2.1.1. The Longevity of Anthropogenic CO_2

Le Quéré et al. (2009) showed that "between 1959 and 2008, 43% of each year's CO_2 emissions remained in the atmosphere on average; the rest was absorbed by carbon sinks on land and in the oceans" (p.831). The carbon cycle involves biogeochemical processes that regulate the concentrations of carbon dioxide in the atmosphere on different timescales. The short-term terrestrial carbon cycle processes operate on daily to seasonal timescales and include photosynthesis, respiration and decomposition of organic matter in soils (heterotrophic respiration) (Kump et al., 2010). The marine short-term inorganic carbon cycle includes dissolution of CO_2 in the surface ocean and its transfer from the surface ocean to its interior, which is referred to as solubility pump (IPPC, 2013). In addition, photosynthesis, settling of the organic matter and decomposition lead to transfer of CO_2 and nutrients from the surface to the deep ocean, referred to as biological pump processes, which are balanced by physical processes that bring the nutrients back to the surface (i.e. upwelling) (Kump et al., 2010).

The long-term carbon cycle processes include dissolution of calcium carbonate ($CaCO_3$) in ocean sediments (carbonate compensation), which becomes important on millennial timescales. As the ocean takes up more CO_2, its acidity increases, releasing $CaCO_3$ from the deep sediments that increase ocean alkalinity, increasing the ocean's potential to take up more CO_2 (Eby et al., 2009). The sedimentary rocks on land may

undergo weathering processes, taking up CO_2 from the atmosphere, which is relevant on timescales of 10,000-100,000 years (Kump et al., 2010).

Thus, the emitted anthropogenic CO_2 can be taken up by land and dissolved in the surface ocean on different timescales: short (daily to seasonal) and long (millennial) (Archer et al., 2007; Eby et al., 2009). The time needed for the natural carbon sinks to absorb a given fraction of CO_2 is strongly dependent on the cumulative amount of CO_2 emitted (Eby et al., 2009). For amounts of CO_2 emitted instantaneously into the atmosphere (emission pulse) below 1000 GtC, 50% of the atmospheric CO_2 is dissolved in the ocean water on centennial timescales, while close to 30% is neutralized by chemical processes (involving dissolution of $CaCO_3$ in sediments) on millennial timescales (Archer et al., 1997; Eby et al., 2009). For CO_2 emission pulses greater than 1000 GtC, the time to absorb 50% of emitted CO_2 increases to approximately 500 years, and in the case of emission pulses of a size of the fossil fuel reserves (approximately 5120 GtC), more than 2000 years are necessary to absorb 50% of the anthropogenic CO_2 emitted (Eby et al., 2009). Figure 1 illustrates the decay of atmospheric CO_2 for a pulse size of 2560 GtC (light blue curve), where the significant uptake by the ocean (between 1000 and 2000 GtC) occurs after 500 years (dark blue curve).

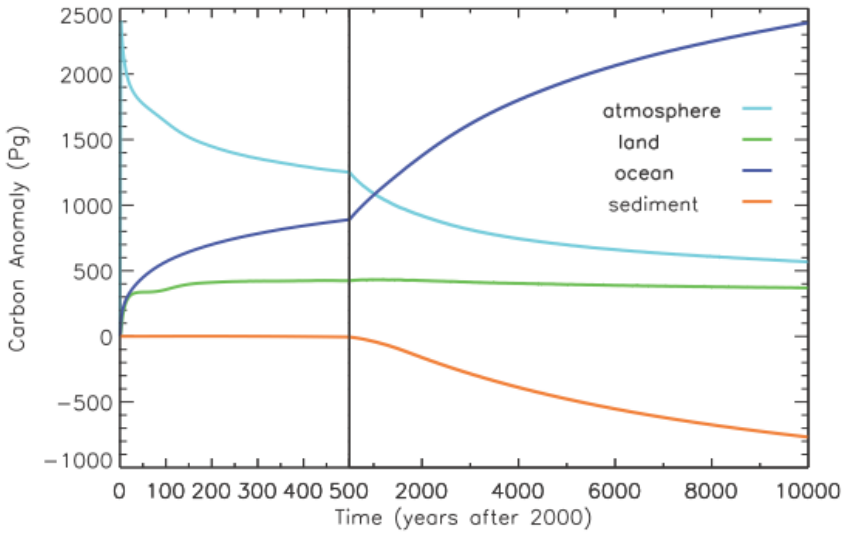

Figure 1. Temporal changes in carbon pools
Changes in carbon pools for a CO_2 emissions pulse of 2560 GtC. Note: 1PgC = 1GtC. ©American Meteorological Society. Used with permission. Citation: Eby, M., Zickfeld, K., Montenegro, A., Archer, D., Meissner, K. J., & Weaver, A. J. (2009). Lifetime of anthropogenic climate change: Millennial time scales of potential CO_2 and surface temperature perturbations. Journal of Climate, 22(10), 2501-2511. doi: 10.1175/2008JCLI2554.1

Because of the longevity of CO_2 in the atmosphere, the CO_2 emitted by fossil fuel combustion processes causes climate perturbations for thousands of years into the future (Archer et al., 2009; Eby et al., 2009). Evidence for such behaviour is found in the sedimentary records from the deep past during the Palaeocene-Eocene thermal maximum (Archer et al., 2009), when the recovery from sharp increases in the atmospheric CO_2 during that period took approximately 150,000 years (Archer et al., 2009).

2.1.2. Delayed Warming of the Climate System

The delay in the climate's system response to radiative forcing is known as thermal inertia (Hansen et al., 2005). The primary reason for the existence of thermal inertia is the large heat capacity of the ocean, which is the primary reservoir of surplus energy (Hansen et al., 2005). A warmed ocean slowly releases heat back to the atmosphere on long timescales (centennial to millennial). Because of thermal inertia, the climate system does not equilibrate instantly with a given level of radiative forcing. According to Hansen et al. (2005), at least 25 to 50 years are required to reach 60% of

the equilibrium response for the Earth's surface temperature (Hansen et al., 2005) and it takes several centuries to millennia to reach the full equilibrium response. Thus, even if the atmospheric composition was stabilized at current levels, inevitable additional global warming of 0.6˚C is predicted to occur in the future (Hansen et al., 2005).

2.2. Irreversibility of CO_2-induced Climate Change

As defined by Boucher et al. (2012), irreversibility implies that "the system cannot be restored to its initial state or only does so on a timescale far longer than those normally considered practical from a human perspective" (p.3). Irreversibility could arise due to hysteresis behaviour, defined as the dependence of the climate system response not only on its current state but also on its history, and due to a lag between the input and output variables (for example, delayed warming due to ocean thermal inertia) (Boucher et al., 2012).

Climate change after a complete cessation of the CO_2 emissions is irreversible on centennial timescales (Matthews & Caldeira, 2008; Zickfeld et al., 2012), or even up to 1000 years after the cessation of emissions (Eby et al., 2009; Frölicher and Joos, 2010; Gillett et al., 2011; Lowe et al., 2009; Solomon et al., 2009). These studies indicate that a complete cessation of CO_2 emissions leads to an approximately constant global mean temperature for several centuries. This constancy arises because after cessation of emissions, the decrease in radiative forcing due to declining atmospheric CO_2 levels is counterweighed by a slow release of heat from the ocean (Eby et al., 2009; Zickfeld et al., 2013).

Gillett et al. (2011) performed a set of experiments with cessation of emissions at different years. Although complete cessation of emissions leads to stabilization of the global mean temperature, the sea level continues to rise for centuries onward. The resulting temperature response and thermosteric sea level rise (i.e. the component of sea level rise due to thermal expansion of the ocean) are presented in Figure 2.

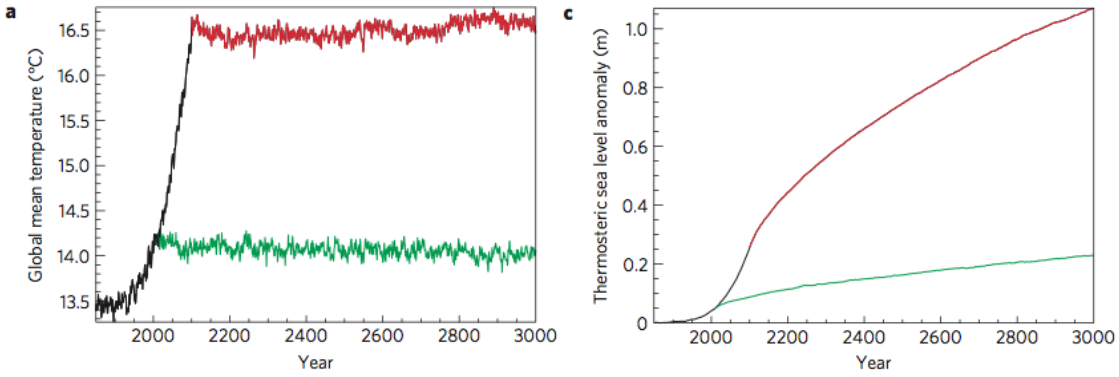

Figure 2. Time series of the climate response to cessation of CO_2 emissions
CO_2 emissions follow historial values until year 2010, and the A2 scenario from the Special Report on Emissions Scenarios (SRES; IPCC, 2007). In the first experiment (green pathway) emissions cease in year 2010, while in the second experiment (red pathway), emissions cease in year 2100. The black line represents the response to historical and A2 scenario CO_2 emissions. Reprinted with permission from Gillett et al. (2011).

Furthermore, while the global mean temperature remains constant for many centuries after cessation of CO_2 emissions, the on-going regional changes in temperature are substantial (Gillett et al., 2011). Other irreversible changes discussed in the literature include melting of permafrost and glaciers, in addition to increase in the frequency and intensity of heavy rainfall and intense hurricanes (Solomon et al., 2009)

2.3. Climate Response to Artificial Atmospheric CO_2 Removal

Held et al. (2010) and Cao & Caldeira (2010) investigated the temperature response to a scenario where the atmospheric CO_2 is instantaneously returned to pre-industrial levels. Also, Boucher et al. (2012) examined the degree of reversibility of the Earth System components under idealized scenarios, where the atmospheric CO_2 concentration increases at 1% per year to the target level (up to 4 times above the pre-industrial CO_2 concentration) and then declines at the same rate to the pre-industrial level.

The results of these studies can be generalized to show that while the mean land surface temperature responds promptly to the decrease in CO_2 concentrations, temperature over the ocean as well as thermosteric sea level (driven by thermal

expansion of the ocean) exhibit a time lag (Boucher et al., 2012). Globally, the decline in atmospheric CO_2 does not result in a simultaneous decrease in temperature to preindustrial levels, as the heat stored in the oceans continues to be released for centuries onwards (Held et al., 2010; Cao & Caldeira, 2010). Other climate system components, such as global sea ice area, also exhibit a lag in their responses, as they follow the temperature trajectory (MacDougall, 2013). With a large amount of CO_2 artificially removed from the atmosphere (up to 5000 GtC removed over the next few centuries), the meridional overturning circulation recovers above pre-industrial levels and thermosteric sea level reverses and starts to decline (MacDougall, 2013).

The scenarios considered in the Cao and Caldeira (2010) study assume instantaneous removal of all anthropogenic CO_2, which currently would not be feasible. Similarly, the 1% per year decrease in atmospheric CO_2 in the Boucher et al. (2012) study is likely unrealistic, as it would require very high rates of negative emissions (up to -30 GtC/year) over the next two centuries. MacDougall's (2013) study focuses on "mirrored" CO_2 concentration pathways with respect to the concentration peak, which are not plausible either, as they do not account for the constraints related to the implementation of artificial atmospheric CO_2 removal at technologically feasible rates. In addition, some of the scenarios would require extremely large amounts of negative emissions, close to 5000 GtC removed over the next few centuries (MacDougall, 2013).

The novelty of our research lies in exploring the physical and biogeochemical climate response to plausible CO_2 emission pathways that meet technological constraints regarding implementation of negative emissions (Section 3.3.1) and follow a smooth transition from a fossil fuel based economy to a zero-emission energy system over the next hundred years.

2.3.1. Net-negative Emission Technologies

Several technologies are being discussed to remove CO_2 from the atmosphere. Due to on-going research and development in this area, such technologies include, but are not limited to, capturing CO_2 directly from the air, biomass combustion with carbon capture and storage (bioCCS), biochar, and enhancing natural carbon sinks. This

section presents a brief overview of these four net-negative CO_2 emission technologies, and discusses the limitations of implementing them on a large scale.

General Direct CO_2 Capture From the Air

Direct air capture typically occurs in a scrubbing tower, where air is vented at the bottom of the tower and undergoes chemical scrubbing process (for example via the soda-lime process, which uses aqueous sodium hydroxide as an absorbent; McGlashan et al., 2012) to separate CO_2 from air and output clean air at the top of the tower. The pure captured CO_2 can be transported and stored in geological formations, similar to the ones used in carbon capture and storage (CCS) technology (Keith et al. 2006; McGlashan et al., 2010; Workman et al., 2011). The major cost is not the capture process itself but the energy-intensive recovery of the solvents (Lackner, Grimes, & Ziock, 2001; Ranjan & Herzog, 2011). The limiting factors of implementing this technology on a large scale include substantial requirements for energy (heating to required temperature of 900°C) and shipping of lime (necessary input) to appropriate locations, which would require capital investments to build appropriate ships (McGlashan et al., 2012). Interestingly, limitations in availability of limestone or dolomite can be neglected due to abundance of these minerals (McGlashan et al., 2012). Although there are no other physical limits of implementing direct air capture on a large scale (Cao & Caldeira, 2010; McGlashan et al., 2012), the costs related to its implementation and lack of incentive from the government to reduce CO_2 emissions on a large scale prevent from its deployment. Furthermore, the success of direct air capture depends on the development of the reliable carbon capture and storage technologies (CCS) that store concentrated CO_2 in geological structures, possibly without leakages (McGlashan et al., 2012). Global capacity of geological storage (estimated between 572 and 1900 GtC) and regional storage constraints also need to be considered (Tavoni et al., 2013).

Biomass Energy with Carbon Capture and Storage (bioCCS)

Atmospheric CO_2 is naturally removed from the atmosphere through photosynthesis and stored in a form of biomass, which can be combusted with the use of carbon capture and storage (CCS) technologies, to produce energy and result in a net-negative impact on the atmospheric CO_2 concentration (Ranjan & Herzog, 2011). However, the success of the development and implementation of bioCCS on a large

scale is related to the development of regular carbon capture and storage techniques that bioCCS heavily relies on (McGlashan et al., 2012). In addition, implementation of this technology on a large scale is limited by the availability of biomass, as the agricultural land capable of producing biomass is limited by geographical factors. Furthermore, large-scale biomass production for bioCCS purposes raises food security concerns, as it may compete with biomass needed for food production and feedstock supply chains (McGlashan et al., 2012; Ranjan & Herzog, 2011).

Biochar

The process of combustion of biomass in a low oxygen environment creates enriched carbon biomaterial that is referred to as biochar (McGlashan et al., 2012). Such carbon-rich biochar can be stored in landfills or used in agriculture to fertilize land (McGlashan et al., 2012), thereby, locking the carbon in the soil (McGlashan et al., 2010; Workman et al., 2011). However, McGlashan et al. (2010) and Workman et al. (2011) emphasize that further research is needed on the stability of carbon in the biochar. The advantage of biochar technology is that it can be used on a small-scale and is not capital intensive (McGlashan et al., 2010; Workman et al., 2011). However, the amount of biomass available for combustion is the limiting factor for implementing this technology on a large scale.

Enhancing Natural Carbon Sinks

The ocean is one of the largest natural carbon sinks, which could potentially be artificially enhanced to absorb more CO_2 from the air (Ranjan & Herzog, 2011). One approach suggests the addition of lime or alkali that would increase the pH of surface waters, a process often referred to as augmented ocean disposal (McGlashan et al., 2010; Workman et al., 2011). Another approach to increase the capacity of CO_2 storage by the ocean carbon sink is large-scale fertilization that enhances ocean biological productivity (Workman et al., 2011; McGlashan et al., 2010). Not only are significant energy inputs required for this technology (McGlashan et al., 2012), but also the impacts on the marine environment are not fully known (McGlashan et al., 2010; Workman et al., 2011).

2.3.2. Costs of Net-Negative Emission Technologies

McGlashan et al. (2012) examined the costs of net-negative emission technologies based on a full life cycle analysis. Implementation of these technologies is related to financial and energy costs, as well as mineral inputs in some cases (McGlashan et al., 2012). Their results show that the total cost of artificial atmospheric CO_2 removal through the implementation of augmented ocean disposal (\$95/tCO_2) and bioCCS (\$59-111/tCO_2) is substantially lower than those of biochar (\$135/tCO_2) or the direct capture of atmospheric CO_2 through the soda-lime process (\$155/tCO_2) (McGlashan et al., 2012). Interestingly, the costs of biochar and bioCCS could be potentially reduced if a substitute for nitrate-based fertilizers is developed and used on a wide scale with biochar production (McGlashan et al., 2012).

In addition, since the primary goal of bioCCS is to generate power, and the net-negative emissions are just a by-product, this technology may be easier to implement in the current economy system, compared to the technologies which only aim to generate net-negative emissions (McGlashan et al., 2012). However, there are issues related to scaling up bio-CCS based technologies, due to their interference with food supply and land use change impacts (McGlashan et al., 2012).

Chapter 3. Methods

3.1. Introduction to Climate Models

McGuffie and Henderson-Sellers (2000) defined climate models as the "tools employed to enhance understanding of the climate system and to aid prediction of future climates" (p. 1072). Different climate models represent the climate system with various degrees of complexity, from simple zero or one-dimensional energy-balance models (EBMs) and radiative convective models with vertical temperature profiles, to more comprehensive Earth System Models of Intermediate Complexity (EMICs) and complex Earth System Models (ESMs), which are based on General Circulation Models (GCMs) of the ocean and atmosphere (McGuffie & Henderson-Sellers, 2000).

Climate models describe the processes occurring in the Earth's natural system, without the anthropogenic interaction with nature (human behaviour is treated as external driving force) (Brovkin et al., 2009; Claussen, et al., 2002). Although the spatial and temporal resolution are reduced in EMICs, as compared to GCMs and ESMs, EMICs are able to simulate the feedbacks between many components of the climate system (Claussen et al., 2002) and are more efficient computationally (Brovkin et al., 2009). Moreover, EMICs are useful for studying long-term climate changes by performing simulations over several thousands of years (Claussen et al., 2002). Claussen et al. (2002) categorized climate models in terms of three attributes: integration, detail of description and the number of processes (Figure 3). Regarding the number of processes represented and detail of description, EMICs are in between the conceptual and comprehensive models, but they often have a higher level of integration than comprehensive models (Claussen et al., 2002; Figure 3).

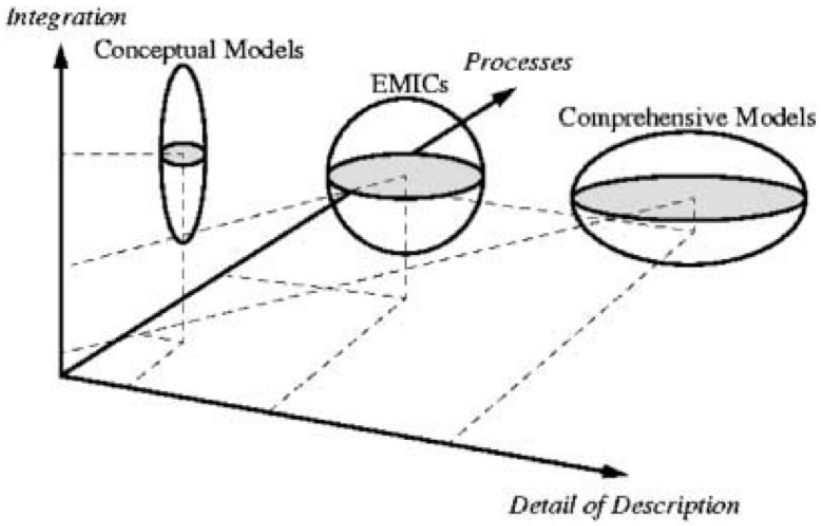

Figure 3. Pictorial definition of EMICs
Reprinted with permission from Claussen et al. (2002).

The advantage of using an EMIC is the ability to simulate the climate over longer timescales (up to thousands of years). While the General Circulation Models (GCMs) are capable of modeling processes with a greater level of detail, their computing time increases with complexity of the model, thereby making it infeasible, in practice, to model processes at timescales longer than a few hundreds of years. Another advantage of models of intermediate complexity is the ability to perform sensitivity analysis and explore multiple parameter settings for different emission pathways with acceptable computational costs.

3.2. The University of Victoria Earth System Climate Model

The University of Victoria Earth System Climate Model (UVic ESCM) is a model of intermediate complexity with a horizontal grid resolution of 1.8˚(meridional) x 3.6˚(zonal) (Weaver et al., 2001). The physical model consists of an atmosphere model coupled to an ocean general circulation model (including both organic and inorganic carbon cycle), a sea ice model and a land surface model together with terrestrial vegetation (Weaver et al., 2001). Each of the model components is described in the following sections.

3.2.1. The Atmosphere Component

The atmosphere is represented by a single layer energy-moisture balance model, as specified by Equation 1 below. The thermodynamic energy-balance equation is vertically integrated, assuming that temperature and specific humidity decrease exponentially with height (Weaver et al., 2001). Atmospheric heat and moisture transport is parameterized by diffusion and advection by winds (Weaver et al., 2001).

The vertically integrated atmospheric energy balance equation is given by:

$$\rho_a h_t c_{pa} \frac{\partial T_a}{\partial t} = Q_T + Q_{sW} C_A + Q_{LH} + Q_{LW} + Q_{SH} - Q_{PLW} \quad (1)$$

Equation 1. Thermodynamic energy balance equation in the UVic model

The left-hand side of Equation 1 consists of constant surface air density (ρ_a), constant scale height for temperatures (h_t), specific heat of air at constant pressure (c_{pa}), and a partial time derivative of the surface air temperature (T_a). The right-hand side components of the vertically integrated energy balance include heat transport (Q_T ; parameterized by Fickian diffusion), incoming shortwave radiation at the top of the atmosphere ($Q_{SW}C_A$; which is a function of the annual distribution of solar insolation at the top of the atmosphere and albedo, and depends on the latitude and time of year), latent heat flux into the atmosphere (Q_{LH} ; for both snow and rain), planetary long wave radiation (Q_{LW} ; emitted by Earth's surface and absorbed by the atmosphere;), sensible heat flux (Q_{SH}; dependent on the speed of wind) and outgoing planetary long wave radiation (Q_{PLW}) (Weaver et al., 2001).

Equation 2 represents the vertically integrated moisture balance, where E is evaporation, P stands for precipitation or sublimation, q_a is the surface specific humidity, and k is eddy diffusivity:

$$\rho_a h_t \left\{ \frac{\partial q_a}{\partial t} - \nabla \cdot (k \nabla q_a) \right\} = \rho_o (E - P) \quad (2)$$

Equation 2. Moisture balance equation in the UVic model

The atmosphere model is reduced in complexity, compared to general circulation models, to make the model more computationally efficient (Weaver et al., 2001). As a

result, the model does not include atmospheric dynamics. Wind fields are specified from observed data, although dynamical wind feedbacks are also included as an option (Weaver et al., 2001).

3.2.2. Ocean Model

The atmospheric model is coupled to a three-dimensional ocean general circulation model, consisting of 19 vertical levels and global resolution of 1.8˚(meridional) x 3.6˚(zonal) (Weaver et al., 2001). The ocean model is based on the Geophysical Fluid Dynamics Laboratory (GFDL) Modular Ocean Model 2.2 (Weaver et al., 2001), which is governed by conservation of momentum, expressed by the Navier Stokes equations with hydrostatic and Boussinesq approximations, in addition to conservation of mass and energy, as explained below (Weaver et al., 2001). Both organic and inorganic carbon cycles are included in the ocean component of the UVic model.

In the modelled ocean, the friction terms are assumed to be insignificant away from the shores, and as a result, the Coriolis force is equal to centrifugal force (away from the boundaries), which is also known as the geostrophic equilibrium. Furthermore, since the terms representing the pressure gradient force and the force due to gravity are much greater compared to other vertical terms, the hydrostatic approximation assumes that other vertical terms are insignificant and sets the force due to gravity equal to the vertical pressure gradient force (Pond & Pickard, 1995). The Boussinesq approximation assumes that the differences in densities are insignificant unless they are multiplied by the acceleration due to gravity.

Inorganic Ocean Carbon Model

The Inorganic Ocean Carbon model is represented by Ocean Carbon-Cycle Model Intercomparison Project (OCMIP) abiotic protocols (Orr et al., 1999). The model includes the ocean carbonate chemistry to determine the atmosphere-ocean flux through the CO_2 content in surface waters (Ewen et al., 2004). The dissolved inorganic carbon (DIC) is also influenced by changes in precipitation, evaporation and runoff (Weaver et al., 2001). In addition, the UVic model also includes a module representing ocean

sediment carbon storage model, which impacts the results of the ocean carbon cycle on millennial timescales (Eby et al., 2009).

Organic Ocean Carbon Model

The organic carbon cycle model includes an Ocean Ecosystem Biogeochemical Model (OEBM), represented by nutrient, phytoplankton, zooplankton and particle detritus (NPZD) (Schmittner et al., 2005). The ecosystem model includes two types of particle detritus: particulate organic detritus (sinking to deeper levels and quickly remineralizing) and dissolved organic matter that does not sink and remineralizes at a slower rate (Schmittner et al., 2005). The ocean ecosystem model simulates biological carbon uptake, nitrate and nutrient availability as well as the effects of light penetration (Friedlingstein et al., 2006; Weaver et al., 2001). While the ecosystem model represents the nitrogen cycling, it does not explicitly account for iron limitation (Schmittner et al., 2005). The growth rate of phytoplankton is limited by the amount of solar irradiance and the availability of nutrients. The light-saturated growth depends only on the temperature, while the light-limited growth depends on the shortwave radiation at a given depth (Schmittner et al., 2005).

Thermodynamic-Dynamic Sea Ice

The ocean general circulation model is coupled to a sea-ice model (Weaver et al., 2001). The sea ice model includes thermodynamic components (open water sea ice and its changing area) as well as dynamic components governed by momentum balance, which responds to oceanic and atmospheric (wind) stresses (Weaver et al., 2001).

3.2.3. Land Surface Model with Dynamic Vegetation

The UVic model also includes a land surface model coupled to a terrestrial vegetation model, represented by “a simplified version of the Hadley Centre Met Office Surface Exchange Scheme (MOSES) coupled to the Top-down Representation of Interactive Foliage and Flora Including Dynamic vegetation model” (TRIFFID; Eby et al., 2009, p.2502; Meissner et al., 2003).

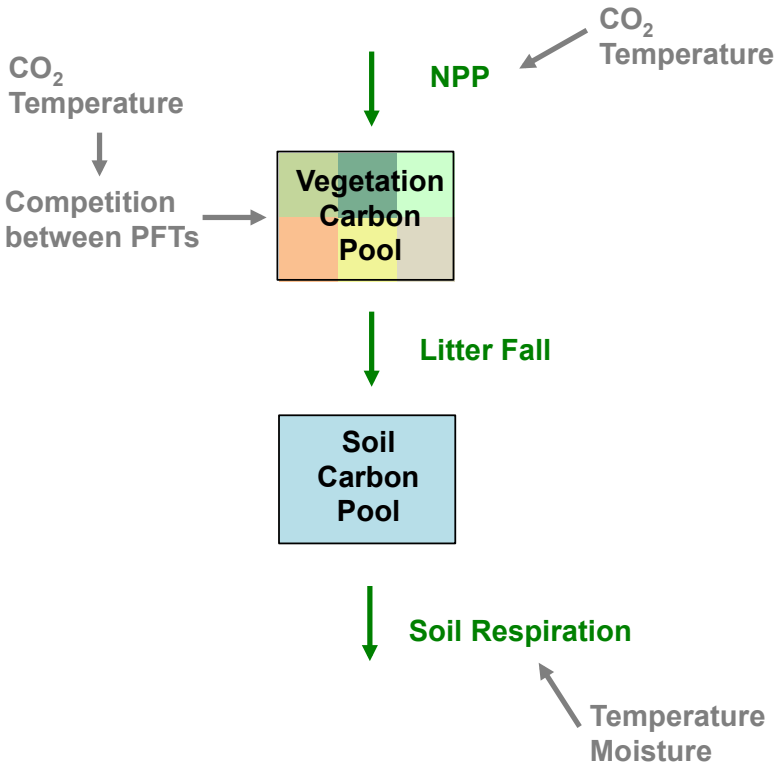

Figure 4. Schematic representation of carbon pools and carbon fluxes in the UVic model

Green arrows represent fluxes between the carbon pools (black framed boxes), while grey arrows indicate drivers influencing carbon pools and fluxes. Five Plant Functional Types (PFTs; represented by different coloured tiles in the Vegetation Carbon pool) are present in the dynamic vegetation model, which include: broadleaf forest, needleleaf forest, C3 grass, C4 grass and shrub. Net Primary Productivity (NPP) is derived separately for each PFT.

The terrestrial carbon uptake is calculated by changes in vegetation and soil carbon storages, which are driven by NPP and soil respiration fluxes, respectively, and interconnected by litter fall, as indicated in Figure 4. Vegetation mortality and litter fall transfer carbon between the vegetation and the soil, where temperature and moisture influence decomposition of soil carbon (Figure 4). The resulting flux of carbon from the soil to the atmosphere is referred to as soil respiration (Friedlingstein et al., 2006). Planetary albedo, roughness length and conductance of stomata are determined by vegetation coverage, thereby influencing water availability and heat fluxes between land and atmosphere (Friedlingstein et al., 2006).

Net primary productivity (NPP), defined as the difference between photosynthesis (vegetation taking up CO_2, when light is available) and dark respiration (vegetation releasing CO_2, without light), drives changes in the vegetation carbon storage (Friedlingstein et al., 2006). The factors influencing NPP include atmospheric CO_2 concentration levels, temperature, light, humidity, soil moisture and availability of nutrients (Friedlingstein et al., 2006). Terrestrial carbon feedbacks due to increased CO_2 levels (CO_2 fertilization, a negative feedback), and weakening of the carbon sinks driven by the increase in the temperature (positive feedback) are also included (Matthews & Caldeira, 2008).

The vegetation model represents five different plant functional types (PFTs): broadleaf tree, needle leaf tree, C3 grass, C4 grass and shrubs (Weaver et al., 2001). Changes in temperature and atmospheric CO_2 concentration drive changes in vegetation distribution. The vegetation fraction for each functional plant type is calculated based on Lotka-Volterra competition equations (Meissner et al., 2003).

The TRIFFID model is coupled to a land surface model, which uses a single soil layer model to define land surface, soil and skin temperature and moisture availability (Meissner et al., 2003). The land surface model also calculates the energy balance for the bare soil as well as for each functional plant type (Meissner et al., 2003).

Ice sheets and land-based ice dynamics are not included in this version of the UVic model.

3.2.4. Level of Sophistication of the UVic Model Components

While EMICs are capable of capturing essential processes and feedbacks in the climate system, they may have a reduced complexity of some of their components or lower resolutions relative to complex Earth Systems models (Eby et al., 2013). Table 1 demonstrates the placement of the UVic model among other EMICs with regards to the level of sophistication of particular model components.

Table 1. **Main features of the EMICs assessed in the AR5, including components and complexity of the models. Model complexity for four components is indicated by colour shading.**

Model name		Atmos	Ocean	Land Surface	Sea Ice	Coupling	Biosphere	Ice Sheets	Sediment & Weathering
Bern3D	Switzerland								
CLIMBER2	Germany								
CLIMBER3	Germany								
DCESS	Denmark								
FAMOUS	UK								
GENIE	UK								
IAP RAS CM	Russia								
IGSM2	USA								
LOVECLIM1.2	Netherlands								
MESMO	USA								
MIROC-lite	Japan								
MIROC-lite-LCM	Japan								
SPEEDO	Netherlands								
UMD	USA								
Uvic	Canada								

Increasing Complexity (light to dark)					
EMBM	2-Box	NST/NSM			None
SD	Q-flux ML	LST/NSM			BO
QG	FG	LST/BSM			BO,BT
PE	PE	LST/CSM			BO,BT,BV

Note: The UVic model is presented in the last row of the table. Darker colour shades represent more complex representation of the specific model component. Reprinted with permission from the IPCC Fifth Assessment Report, Working Group I, Chapter 9, Figure 9.2. Reference: Flato et al., (2013).

Compared to other EMICs, the UVic model ranks high with regards to the complexity of the ocean, land surface and biosphere components (Table 1). On the other hand, the atmosphere component is on the low end of complexity, compared to other EMICs. Sea ice and sediment and weathering components are also included in the UVic model, while not all EMICs include them (Table 1).

3.2.5. Validation of the UVic Model Responses

To validate the accuracy of the climate model responses, the climate and carbon cycle responses can be compared with historical observations (Eby et al., 2013), and with responses of other EMICs, according to different metrics defined further in this section.

Comparing Model Responses with Historical Observations

Surface air temperature anomalies simulated by the UVic model fall within the uncertainty envelope of the observed surface air temperature for the period 1850 to 2005 (Eby et al., 2013). However, the UVic model slightly overestimates the thermosteric sea level anomaly and ocean heat content anomaly for that period, as compared to the historical observations (Eby et al., 2013).

Metrics for Model-intercomparison

Equilibrium Climate Sensitivity

Equilibrium climate sensitivity refers to the global mean temperature change once the climate system reaches equilibrium after doubling the atmospheric CO_2 concentration from pre-industrial levels (IPCC, 2013). As specified by the 5th IPCC Assessment Report, the equilibrium climate sensitivity ranges from 2.1°C to 4.7°C for atmosphere-ocean general circulation models from the Coupled Model Intercomparison Project (CMIP5), with estimated model mean of 3.2 ± 1.3° (IPCC, 2013). A similar range of climate sensitivity values is found by Eby et al. (2013) for EMICs, ranging between 1.9°C and 4.0°C. Compared to other EMIC models, the UVic model's equilibrium climate sensitivity is high (3.5°C, compared to the 3.0°C EMIC mean; Eby et al., 2013).

Transient Climate Response

Transient Climate Response is the global mean surface air temperature change at the time of CO_2 doubling in an experiment with an increase in atmospheric CO_2 concentration at a rate 1% per year (IPCC, 2013). The UVic model's transient climate response is slightly warmer than the EMIC mean value (1.9°C for UVic model, compared to 1.8°C EMIC mean and 0.8°C to 2.5°C EMIC range; Eby et al., 2013). Similarly, the estimated transient climate response for CMIP5 atmosphere-ocean general circulation models is 1.8 ± 0.6°C (IPCC, 2013).

Transient Climate Response to Carbon Emissions

Another metric used for model-intercomparison is the Transient Climate Response to Cumulative Carbon Emissions (TCRE), defined as ratio of global mean surface air temperature change to cumulative CO_2 emissions (Gillett et al., 2013).

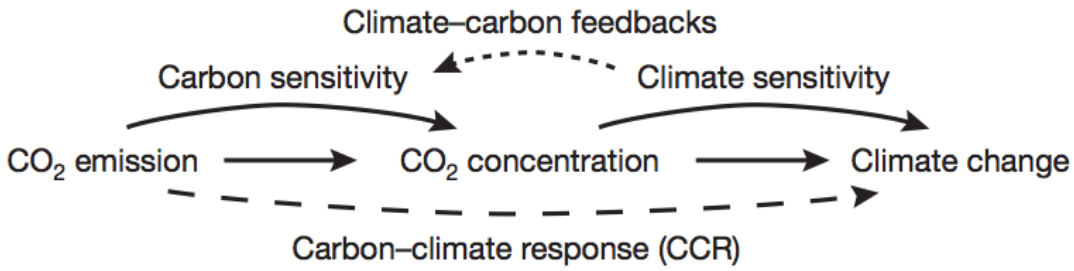

Figure 5. Schematic representation of the progression from CO_2 emissions to climate change

Reprinted with permission from Matthews et al. (2009). Note: Carbon-climate response (CCR) is equivalent to the TCRE measure defined in this section.

The TCRE measure directly captures the impact of CO_2 emissions on climate change, aggregating the impacts of carbon and climate sensitivity into one measure (Matthews et al., 2009; Figure 5). The climate sensitivity measure (defined in the previous section) quantifies the warming per unit change in atmospheric CO_2 concentration, while the carbon sensitivity measures the CO_2 concentration change per unit CO_2 emission (Matthews et al., 2009). The TCRE measure also includes feedbacks between the carbon cycle and climate change (Matthews et al., 2009). Individual measures aiming to quantify the carbon cycle feedbacks alone are presented in the following section.

For an idealized experiment with 1% increase of atmospheric CO_2 concentration up to quadrupling the pre-industrial levels, the UVic model's TCRE is close to the EMIC mean (1.48°C/Eg for UVic model, compared to 1.57°C/Eg EMIC mean and 1.07°C/Eg to 2.21°C/Eg EMIC range; Eby et al., 2013; Note: 1Eg = 1000 GtC).

Carbon Cycle Feedback Parameters

The response of the land and ocean carbon pools as atmospheric CO_2 concentration changes can be quantified by carbon-concentration feedback parameter, while the response to other climate variables such as temperature change can be quantified by carbon-climate feedback parameters (Arora et al., 2013).

The change in land (L) carbon or ocean (O) carbon with respect to change in atmospheric CO_2 concentrations can be expressed in terms of feedback parameters β_L or β_O, respectively (Friedlingstein et al., 2006). Correspondingly, the change in land carbon or ocean carbon with respect to change in surface air temperature can be expressed by feedback parameters γ_L or γ_O, respectively. Compared to other EMICs, the UVic model has high values for β_L (1.09 GtC/ppm, as compared to EMIC mean 0.69 GtC /ppm) and low values for γ_L (-81.6 GtC /ºC, as compared to EMIC mean -61.5 GtC /ºC). On the other hand, for the ocean feedback parameters, the UVic model has somewhat low values for β_O (0.82 Gt/ppm, as compared to EMIC mean 0.92 Gt/ppm) and high values for γ_O (-7.8 Gt/ºC, as compared to EMIC mean -9.6 Gt/ºC) (Eby et al., 2013; Note: 1Pg = 1Gt).

The representation of carbon cycle processes differs widely between models, particularly for the land. For instance, some models include carbon release from peat lands and permafrost, while others include nitrogen limitation (Zickfeld et al., 2013).

3.3. Designing Emission Pathways

For the scope of this research, the UVic ESCM model is driven with CO_2 emission pathways, which are designed to meet feasibility constraints discussed in Section 3.3.1. The model converts CO_2 emissions into CO_2 concentrations and computes the climate and carbon cycle responses (Matthews & Caldeira, 2008). Previous studies exploring the climate response to negative emissions (e.g. Cao & Caldeira, 2010; Boucher et al., 2012; MacDougall, 2013) use idealized pathways and did not consider constraints related to implementation of negative emissions at technologically feasible rates.

To design realistic future emission pathways, information about the possible values and timings of the emission peaks, amount of negative emissions that could be implemented and the rate of emission reduction compatible with plausible rates of decarbonisation of the energy system were derived from the integrated assessment literature, which provides constraints on technical feasibility, as well as economic, political and social factors (Rogelj et al., 2011). The specific constraints used that were used in designing the emission pathways are discussed in the following section.

3.3.1. Emission Pathway Constraints

To ensure the plausibility of CO_2 emission pathways used in this study, we designed them to meet four constraints derived from the integrated assessment literature, which are explained below and summarized in Table 2.

Firstly, to allow for a smooth transition from a current fossil-fuel based economy to a zero-emission energy system while reaching the 2ºC temperature stabilization target, fossil fuel CO_2 emissions are required to peak between 2020 and 2030 and reach zero-emission level by 2100 (Elzen et al. 2010). If the peak occurs at a later time, the rate of emission reductions required would be too high and beyond technological capabilities (too steep reductions required). Also the emission reductions required to reach a zero-emission energy system by 2100 would be very costly.

Secondly, the maximum rate of CO_2 emission reductions is limited to 6% (with respect to year 2000-level, including fossil fuel emissions only), as the rates of reduction beyond 6% are considered extreme (Elzen et al. 2010). The maximum rate of CO_2 emission reductions is constrained by technological progress in developing clean energy and, potentially, negative emission technologies and the rate of introduction of these technologies to the current energy system.

Thirdly, the total amount of negative emissions implemented is limited to 550 GtC (Azar et al. 2010); as bioCCS is the most cost-effective way of removing CO_2 from the atmosphere (Kriegler et al., 2013; McGlashan et al., 2012; Tavoni et al., 2013) and it imposes constraints related to the maximum amount of biomass available to take up atmospheric CO_2, so that there is enough biomass left available for live stock and food

production. The maximum total negative emissions given in the literature ranges from 136 GtC (Tavoni et al., 2013) to 550 GtC (Azar et al., 2010).

Table 2. Constraints used in designing emission pathways

Constraint	Details	Reference
Year of peak emissions	2020 - 2030	Elzen et al., 2010
Maximum rate of CO_2 emissions reduction	< 6%	Elzen et al., 2010
Total amount of negative emissions implemented	<550 GtC	Azar et al., 2010

3.3.2. Future Emission Pathways

We designed two sets of emission pathways: Constant Cumulative Emissions (CCE) and Variable Cumulative Emissions (VCE) pathways. Following the constraints outlined above, the fossil fuel emissions are designed to peak within the next few decades (2018-2030) and decline to zero at a rate no larger than 6% by the year 2100, followed by implementation of negative emissions in the period 2100-2200.

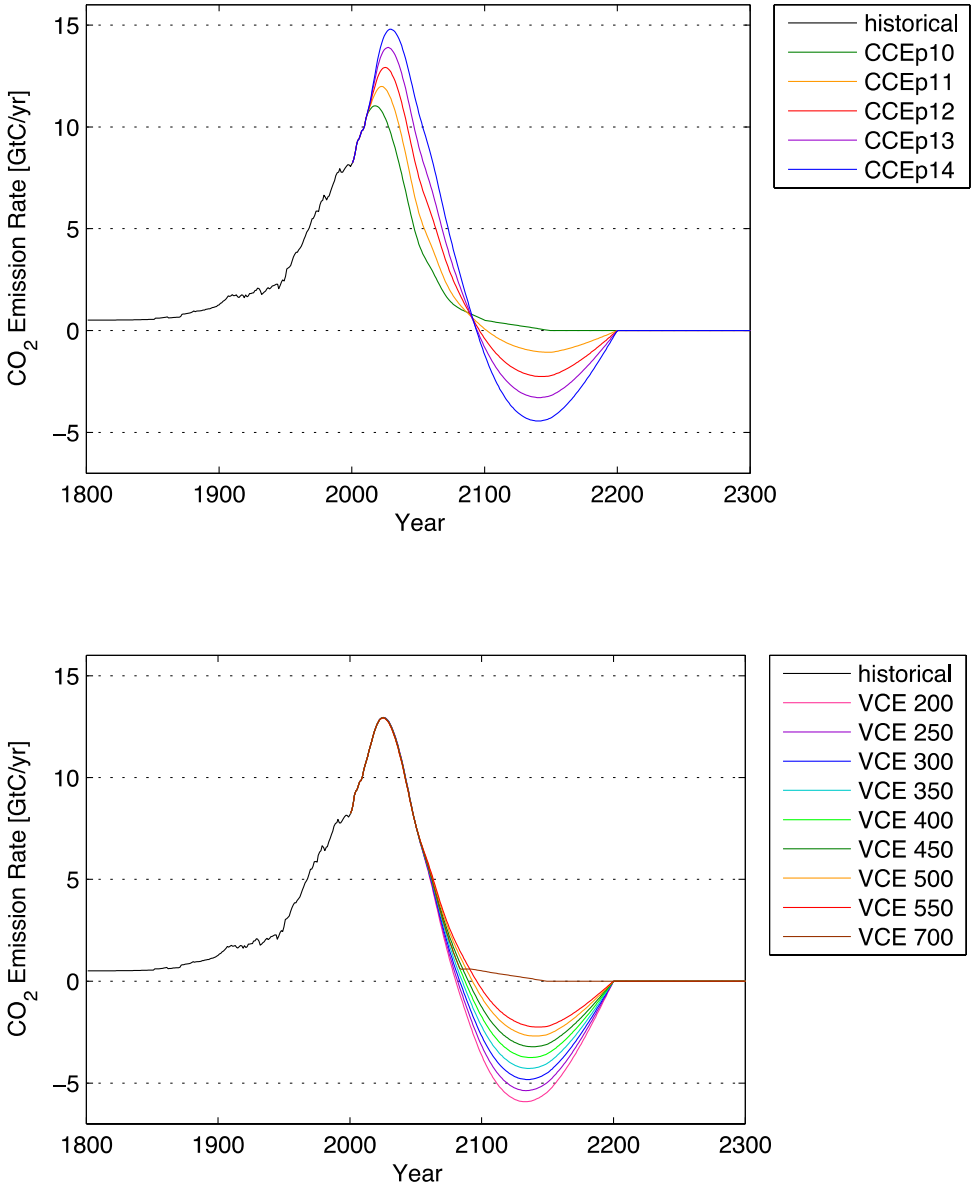

Figure 6. Emission pathways for CCE and VCE simulations
Time series of CO_2 emission rate for simulation CCE (panel a) and for simulation VCE (panel b). The black curve in both panels shows observed historical CO_2 emissions.

Table 3. Emission pathway details

Experiment Name	Simulation Name	Cumulative Emissions GtC	Cumulative Negative Emissions GtC	Peak Fossil Fuel Emission Rate GtC/year	Year of Peak Emission Rate	Maximum Rate of Emission Reduction %
CCE						
	CCEp10	551	0	10	2017	-3.6
	CCEp11	551	-66	11	2022	-4.0
	CCEp12	551	-151	12	2025	-3.9
	CCEp13	551	-224	13	2027	-4.0
	CCEp14	551	-305	14	2029	-4.0
VCE	VCE 200	208	-456	12	2025	-4.3
	VCE 250	258	-410	12	2025	-4.2
	VCE 300	308	-364	12	2025	-4.2
	VCE 350	358	-318	12	2025	-4.1
	VCE 400	408	-273	12	2025	-4.1
	VCE 450	458	-229	12	2025	-4.0
	VCE 500	508	-186	12	2025	-4.0
	VCE 550	551	-151	12	2025	-3.9
	VCE 700	703	0	12	2025	-4.1

Table columns explanation: Column 1: Experiment name; Column 2: Simulation name; Column 3: Total (fossil fuel and LUC) cumulative emissions over the period 2001-2500; Column 4: Total (fossil fuel and LUC) negative emissions; Column 5: Peak emissions rate (fossil fuel emissions only); Column 6: Year of peak emission rate (fossil fuel emissions only); Column 7: maximum rate of emission reduction calculated with respect to year 2000-level (fossil fuel emissions only).

The CCE pathways differ in the peak emissions rate and, accordingly, the amount of negative emissions implemented, to reach the same cumulative emission target (Figure 6 a). The VCE pathways entail the same peak emission rate but different amount of negative emissions implemented and, hence, different cumulative emission targets are reached (Figure 6 b). Table 3 contains numerical details for both emission pathways.

In both sets of pathways, net-negative emissions are implemented in the period 2100-2200, followed by a complete emission cessation (for the period 2200-2500). Also, both sets include a zero-emission pathway, where emissions are rapidly reduced to zero (at much higher rate than technologically available), and cease without implementation of negative emissions. The trajectories of CO_2 emissions are shown in Figure 6 a,b for pathways CCE and VCE, respectively.

Constant Cumulative Emissions (CCE) Pathways

The cumulative CO_2 emission target for the CCE simulations is 550 GtC (including fossil-fuel and land-use emissions) for the period 2001-2500, to meet the 2°C global mean temperature level (Zickfeld et al., 2013). The CO_2 emission pathways differ in the peak fossil fuel emission rate (between 10 and 14 GtC/year), the year of peak emissions (between 2017-2029), and, accordingly, the amount of negative emissions implemented (up to 305 GtC removed for CCEp14), to reach the same cumulative emission target (Figure 6 a). The name of the pathway indicates peak fossil fuel emissions rate (e.g. CCE 10 peaks at 10 GtC/year of fossil fuel emissions; Table 3).

Variable Cumulative Emissions (VCE) Pathways

The VCE emission pathways peak at 12 GtC/year in 2025 (fossil fuel emissions only), followed by implementation of different amounts of negative emissions (up to 456 GtC removed for VCE 200). The pathways reach different amounts of cumulative emissions over the period 2001-2500, in the range of 200-700 GtC (Figure 6 b). The name of each pathway indicates its cumulative emission target (e.g. VCE 200 has cumulative emissions of 200 GtC). Table 3 contains detailed information about the parameters for each emission pathway.

3.4. Model Simulations

The CO_2 emission pathways (from CCE and VCE emission pathway groups) described above were used to drive simulations with the University of Victoria Earth System Climate Model of intermediate complexity (UVic ESCM 2.9). Simulations also included radiative forcing from sulphate aerosols, non-CO_2 greenhouse gases and volcanic and solar forcing.

Firstly, a historical simulation (for the period 1801-2000) was forced with the observed historical CO_2 concentrations to follow the observed temperature trajectory. The historical run also included observed volcanic and solar forcing for the historical period, and forcing from non-CO_2 greenhouse gases and sulphate aerosols, which also follows observed values. The historical simulation provided initial conditions for the future runs.

Two sets of future model simulations were conducted, driven by CCE and VCE CO_2 emissions pathways, respectively. In all simulations, land-use change (LUC) emissions follow scenario RCP 2.6 (Vuuren et al. 2007) to the year 2100. After 2100, LUC emissions are linearly extrapolated to reach zero in the year 2150 and reach cumulative emissions of 72.1 GtC (for the period 2001-2100). In addition to CO_2 emissions from fossil fuels and LUC, all runs include forcing from sulphate aerosols and non-CO_2 greenhouse gases. Both forcings are stabilized at a constant year-2010 value for future years. Natural forcing due to volcanic eruptions is set to zero for the future simulations, as future eruptions are highly uncertain and difficult to predict.

Although CO_2 emissions cease in year 2200, the simulations were run for additional 300 years (until 2500) to account for lag in the responses of the climate system components.

Chapter 4. Results

4.1. Physical Climate System Responses

4.1.1. CCE Simulations

CCE simulations are forced with CO_2 emission pathways that reach the same cumulative emission target of 550 GtC (since year 2001), equivalent to reaching the 2°C temperature target above the pre-industrial level. In this section, we will compare the climate response of the CCEp14 pathway with the highest peak emission rate (14 GtC/year, fossil fuel emissions) and hence, the largest amount of negative emissions implemented (305 GtC removed), to the response of the CCEp10, which is a zero-emission pathway with a low peak emission rate (10 GtC/year, fossil fuel emissions) and no negative emissions. The climate response to other CCE emission pathways falls between that for these two chosen pathways.

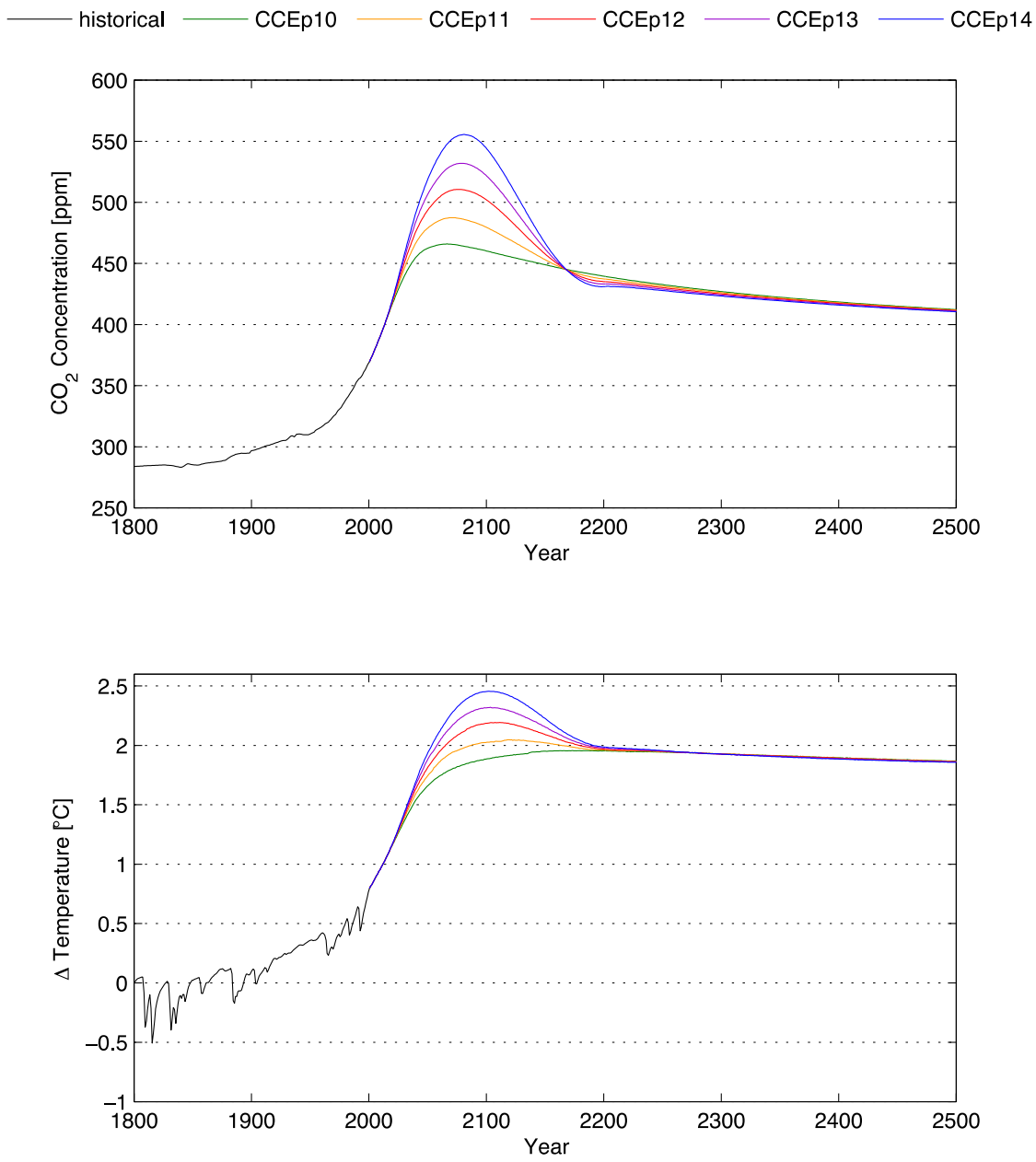

Figure 7. Time series of CO_2 concentration and temperature for CCE simulations

Time series of atmospheric CO_2 concentration (panel a) and temperature change relative to 1801 (panel b). Note: The historical temperature values in panel b represent the model response to the observed historical forcing.

Atmospheric CO_2 Concentration

In the CCE simulations, the atmospheric CO_2 concentration peaks around years 2067-2082 at 466-555 ppm (Figure 7 a), lagging the peak in fossil fuel emissions (2018-2030) by approximately 49-52 years. The lag in the response of the atmospheric CO_2 concentrations to the CO_2 emissions is due to the fact that CO_2 accumulates in the atmosphere and is only partly taken up by terrestrial carbon sinks and the ocean (Le Quéré et al., 2009). The atmospheric CO_2 concentration peaks and declines when the rate of the CO_2 emissions becomes lower than the rate of uptake by the natural terrestrial and ocean carbon sinks.

After the peak, CO_2 concentrations first decline rapidly until year 2190, followed by much slower decrease at later times (until year 2500). Negative emissions implemented in the period 2100-2200 are responsible for the rapid decrease in the CO_2 concentrations, as the rates of decline in CO_2 concentrations are larger for pathways with greater amounts of negative CO_2 emissions (e.g. pathway CCEp14 in Figure 7 a). However, the decrease in CO_2 concentrations starts a few years before the implementation of negative emissions, due to CO_2 uptake by natural carbon sinks (terrestrial biosphere and ocean).

The uptake of the atmospheric CO_2 by terrestrial vegetation through photosynthesis is enhanced at higher atmospheric CO_2 concentrations (referred to as CO_2 fertilization effect), as well as increased temperatures in boreal and temperate regions (Heimann & Reichstein, 2008). Both of these effects saturate at high levels of CO_2 concentrations and high temperatures (Heimann & Reichstein, 2008). This natural carbon uptake by terrestrial carbon sinks is reversed during the negative emissions phase, as the atmospheric CO_2 concentrations decline, and hence, the CO_2 fertilization effect diminishes and the CO_2 partial pressure between the atmosphere and the ocean decreases, thereby decreasing the amount of CO_2 flux driven into the ocean. As a result, the implementation of negative emissions in the period 2100-2200 is opposed by a slow release of CO_2 by these carbon sinks (Section 4.2). Finally, for the period 2200-2500, the atmospheric CO_2 concentrations decline slightly due to natural carbon uptake, especially by the ocean, and converge for all the pathways at year 2200.

Global Mean Temperature

The global mean temperature peaks in years 2102-2174 (Figure 7 b), ranging from 2.0 to 2.5°C (above the 1801 level), for different CCE pathways. The pathways with higher peak emissions (e.g. Figure 6 a; CCEp14) experience higher peak temperatures (Figure 7 b). Also, the rapid decline in the temperature right after the peak is particularly high for emissions pathways with large amounts of negative emissions implemented in the period 2100-2200. After cessation of CO_2 emissions in year 2200, the global mean temperature (Figure 7b) continues to slowly decline, reaching 1.9°C above the 1801 value in year 2500. The slow decline in temperature level after cessation of emissions is consistent with results from earlier studies (Gillett et al. 2011; Matthews & Caldeira, 2008; Solomon et al., 2009).

In the CCE simulations, emission pathways with higher peak CO_2 emissions (e.g. CCEp14) entail implementation of greater amounts of negative emissions later on, to meet the same cumulative emission target for each pathway (550 GtC since year 2001). As a result, the year-2500 temperature stabilizes at the same value, independently of the emission pathway (Figure 7 b). These findings agree with recent research, which shows that the temperature response is pathway independent and depends only on the cumulative emission targets (Allen et al., 2009; Eby et al., 2009; Matthews et al., 2009; Zickfeld et al., 2009; Zickfeld et al., 2012). However, the short-term temperature response before cessation of emissions largely depends on the specific emission pathway, and so does the short-term spatial distribution of temperature.

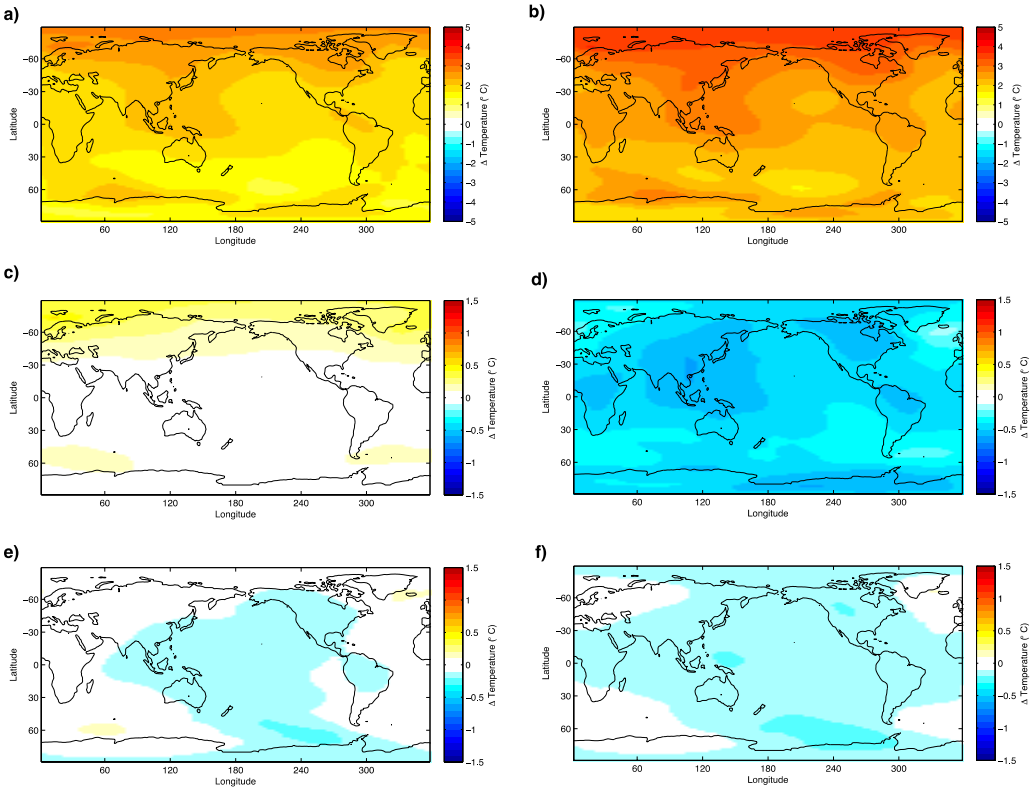

Figure 8. Spatial temperature change for CCEp10 (left) and CCEp14 (right)
Spatial temperature distribution for years a) 2100-1810 for CCEp10; b) 2100-1810 for CCEp14; c) 2200-2100 for CCEp10 d) 2200-2100 for CCEp14; e) 2500-2200 for CCEp10 f) 2500-2200 for VCE CCEp14. Note: Panels have different vertical scales.

Spatial Temperature Distribution

The spatial distribution of surface air temperature (Figure 8) shows that during the positive emission period (until year 2100), the warming at high latitudes is about 2.5°C higher for the high emission pathway (CCEp14) as compared to the reference pathway CCEp10 (with low peak and no negative emissions; Figure 8 a,b). In both cases, northern high latitudes experience greater warming, as compared to other regions, a phenomenon referred to as polar amplification. This occurs due to a positive ice-albedo feedback whereby melting of sea ice and snow cover decreases planetary albedo leading to further warming. In addition, the warming over land is higher than the warming over the ocean due to large heat capacity of the ocean as compared to land.

During the net-negative emission period (years 2100-2200), the negative emissions lower the global mean temperature (up to -1°C change) for pathway CCEp14 (Figure 7 b). Spatially, the cooling occurs mainly in the Tropics, Southern Ocean and the coasts of the Pacific Ocean (Figure 8 c,d). In contrast, the reference pathway CCEp10 (without negative emissions) still experiences slight warming (around 0.5°C) due to thermal inertia of the ocean. These results confirm that implementation of negative emissions is effective in reversing temperature change both globally and spatially on human (centennial) timescales. However, the UVic model does not include some other potentially irreversible processes that could contribute to increasing temperature changes, such as the permafrost feedback and ice sheet mass loss. Melting of permafrost releases large amounts of methane to the atmosphere, which is a strong greenhouse gas that could contribute to global warming. If the UVic model included the permafrost feedback, the attained warming could be higher (MacDougall et al., 2012), and may not be easily reversible on human timescales.

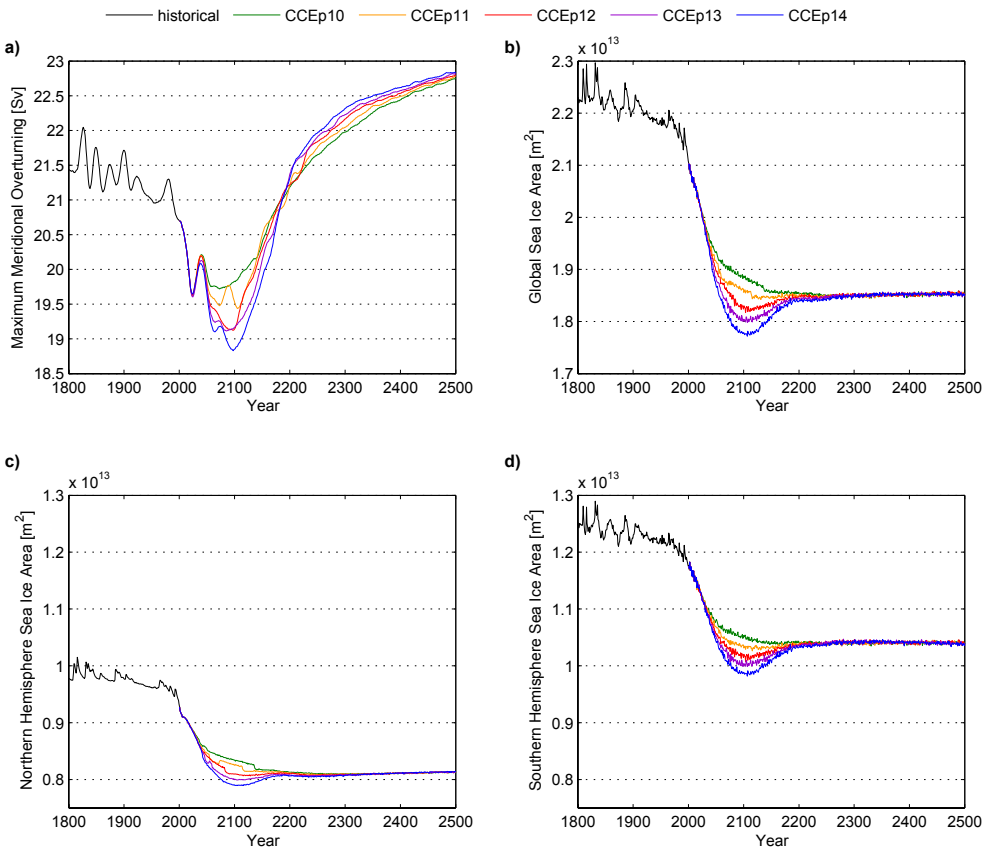

Figure 9. Time series of maximum meridional overturning and sea ice area for CCE simulations (relative to 1801)

Time series of maximum meridional overturning (panel a); global sea ice area (panel b); northern hemisphere sea ice area (panel c); southern hemisphere sea ice area (panel d). Note: The historical values represent the model response to the observed historical forcing.

Sea Ice Area

The increase in the global mean temperature leads to melting of sea ice. The global sea ice area decreases during the positive emission period until year 2100, reaching its minimum value of $1.78 \cdot 10^{13}$ m^2 (20.6% below the year 1801 level) for the highest peak emission pathway CCEp14 (Figure 9 b). The relative decline in sea ice in the Southern Hemisphere (up to 21.6% decline for CCEp14) is similar to that in the Northern Hemisphere (up to 19.3% decline for CCEp14; Figure 9 c,d). During the period of net-negative emissions (2100-2200), the global sea ice area continues to decrease for the reference zero-emission CCEp10 pathway, but recovers for other pathways that entail net-negative emissions (Figure 9 b). After the year 2200, the global sea ice area converges for all pathways and stabilizes at a value of $1.83 \cdot 10^{13}$ m^2 (approximately 17% below the year-1801 level). The recovery of the global sea ice area during the years 2100-2200 is not surprising, as the global mean temperature declines for that period (e.g. by 0.5°C for CCEp14; Figure 7 b). Spatially, the areas of the largest loss of the sea ice (not shown) correspond to the areas of the highest temperature increase in the northern high latitudes

Meridional Overturning Circulation

Warming of the North Atlantic Ocean waters slows down the process of deep-water formation, leading to a weakening of the meridional overturning circulation (also referred to as the thermohaline circulation). Moreover, melting of the sea ice increases the freshwater flux to the ocean and further leads to its weakening. As the sea ice continues to melt until year 2100, the maximum overturning circulation continues to slow down reaching its lowest maximum value at 18.8 Sv for CCEp14 (Figure 9 a). Once the sea ice area starts to recover (during the net-negative emission period), the maximum meridional overturning circulation starts to increase as well. Interestingly, the recovery of the meridional overturning circulating is faster for the pathways with higher emission peaks followed by a larger amount of negative emissions implemented. In year 2500, the maximum meridional overturning circulation reaches values higher than the historical (22.8 Sv for CCEp14; Figure 9 a).

The slowdown of the meridional overturning circulation may be underestimated, as the UVic model does not include dynamic ice sheets. With increased freshwater flux from ice sheet melt, the meridional overturning circulation would slow down even further, which might lead to its collapse in extreme cases.

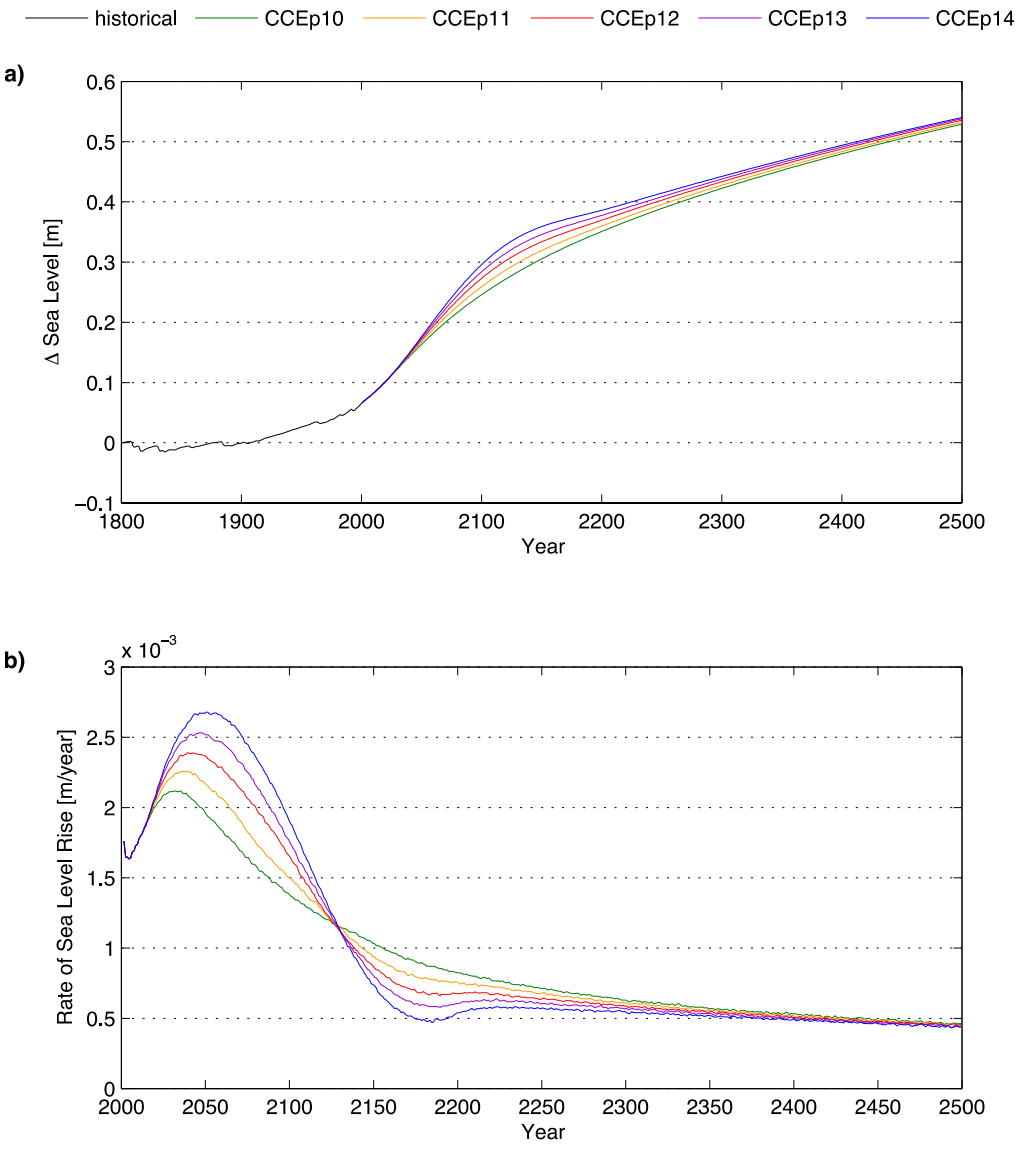

Figure 10. Time series of thermosteric sea level rise and rate of sea level rise for CCE simulations

Time series of the relative thermosteric sea level rise with respect to 1801 (panel a) and calculated rate of sea level rise (panel b). Note: The historical values represent the model response to the observed historical forcing.

Thermosteric Sea Level Rise

During the positive emission phase (until year 2100), the thermosteric sea level rise (due to thermal expansion of the ocean) continually increases for all pathways, and the increase is largest for the pathway with highest CO_2 emission rate (CCEp14; Figure 10 a). Figure 10 b shows rate of change of the relative thermosteric sea level rise with time, which decreases rapidly in the period 2030-2050, once CO_2 emissions start to decline after their peak (Figure 10 b).

Although negative emissions are implemented in 2100, the relative sea level slows down significantly only after 2150 (Figure 10 a). The delayed response of the sea level rise is caused by the thermal inertia of the ocean. Implementation of moderate amounts of negative emissions (up to 305 GtC removed for CCEp14) slows down the rate of sea level rise but does not reverse (Figure 10 b). After cessation of emissions (in year 2200), the thermosteric sea level continues to rise for the CCEp10 pathway (Figure 10 a), which is consistent with other studies, which consider zero emission pathways (Zickfeld et al., 2013). Around year 2200, the rate of sea level rise slightly increases and stabilizes close to 0.5 mm/year (Figure 10 b).

Also, Figure 10 a shows that the thermosteric sea level response in year 2500 not only depends on the amount of cumulative emissions, but also on the specific emission pathway (Figure 10 a), as it is slightly higher for the CCEp14 pathway, as compared to CCEp10 (by 4 cm in year 2200 and by 1cm in year 2500). This result is in agreement with earlier studies (Bouttes et al., 2013; Zickfeld et al., 2012), which showed a slight path dependence of the thermosteric sea level rise on emission pathway.

Our research shows that for the CCE pathways, the sea level rise is not reversible on centennial timescales and continues to increase despite the artificial removal of the CO_2 from the atmosphere. Since the UVic model does not model dynamic ice sheets, our results show only thermosteric sea level rise. If the eustatic sea level rise was included (due to the ice sheet melt), the sea level rise would be even higher and more difficult to reverse due to the long response timescale of ice sheets.

Our second set of experiments, the Variable Cumulative Emissions (VCE) simulations, described in the following section, explores whether the sea level is reversible for larger amounts of negative emissions implemented.

4.1.2. VCE Simulations

The Variable Cumulative Emissions simulations are forced with CO_2 emission pathways that reach different cumulative emission targets (from 200 GtC to 700 GtC; Figure 6 b, Table 3). The reference pathway is VCE 550, which is the same as CCEp12, reaching the 2°C target and entails 305 GtC negative emissions implemented in the period 2100-2200, while the total cumulative emissions since year 2001 are 550GtC (for VCE 550). We will compare this pathway with VCE 200, which entails the largest amount of negative emissions implemented (456 GtC) and reaches a low cumulative emission target of 200 GtC. This comparison will allow us to explore whether the reversibility of climate system components is enhanced if larger amounts of negative emissions are implemented, thereby reaching lower cumulative emission targets. The climate response during the positive emission phase (up to year 2200) for VCE pathways is the same as for the CCEp12 pathway, and hence, the following discussion will focus on the net-negative emission phase (in years 2100-2200).

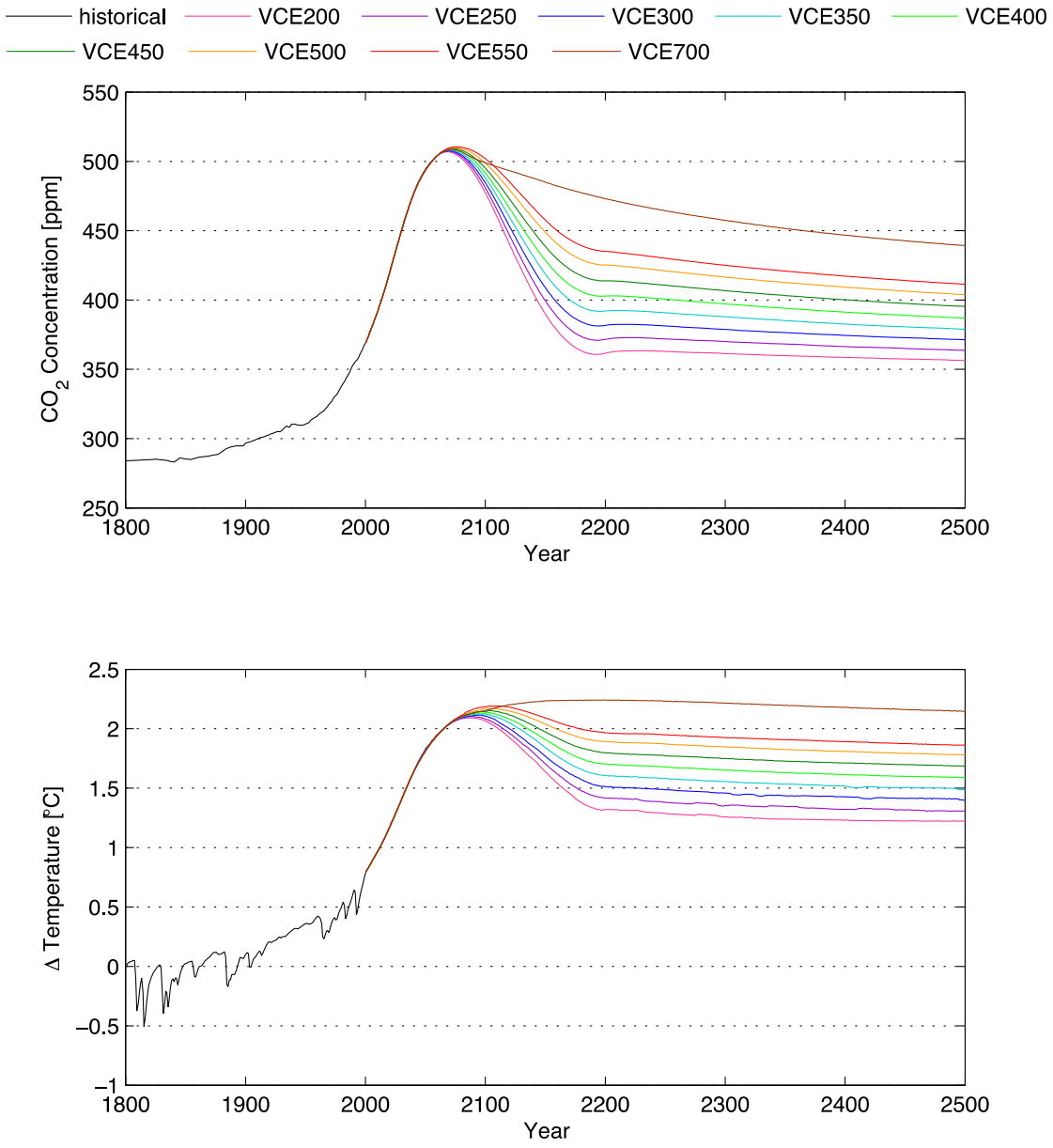

Figure 11. Time series of CO_2 concentration and temperature for VCE simulations

Time series of atmospheric CO_2 concentration (panel a) and temperature change relative to 1801 (panel b). Note: The historical values represent the model response to the observed historical forcing.

The atmospheric CO_2 concentration (Figure 11 a) peaks at a slightly lower value for VCE 200 (507 ppm), as compared to VCE 550 (510 ppm), but this difference is small. Compared to VCE 550, the atmospheric CO_2 concentration declines at a much faster rate for pathway VCE 200 during the net-negative emissions period between 2100 and 2200 (Figure 11 a). The CO_2 concentrations stabilize at a lower level for VCE 200 (356 ppm) compared to VCE 550 (412 ppm) in 2500.

Correspondingly, the global mean temperature (Figure 11 b) peaks at a slightly lower value for VCE 200 (2.1°C) compared to VCE 550 (2.2°C). Subsequently, the global mean temperature (Figure 11 b) declines at a faster rate for VCE 200 compared to VCE 550, and stabilizes at a lower level (1.2°C above the 1801-level, as compared to 1.9°C above the 1801-level). These findings are consistent with the CO_2 concentrations behaviour discussed above (Figure 11 a) and show that the stabilization temperature is lower for pathways with larger cumulative negative emissions. Spatially, during the positive emission phase, the warming is highest in the northern high latitudes region (Figure 12 a,b). Once net-negative emissions are implemented during the period 2100-2200, all regions experience cooling, (stronger in VCE 200 than VCE 550), where the cooling is strongest in the Tropics, the Pacific coastal regions and over the Southern Ocean (Figure 12 c,d).

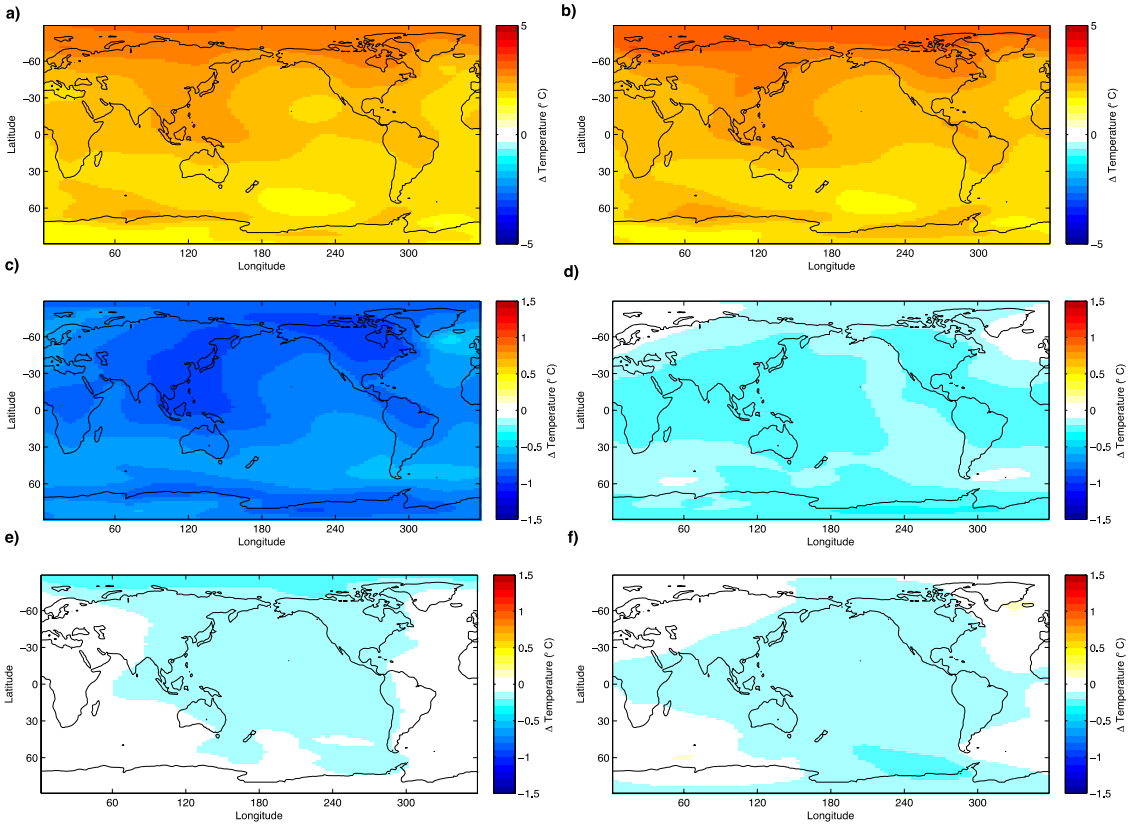

Figure 12. Spatial temperature change for VCE 200 (left) and VCE 500 (right)
Spatial temperature distribution for years a) 2100-1810 for VCE 200; b) 2100-1810 for VCE 550; c) 2200-2100 for VCE 200 d) 2200-2100 for VCE 550; e) 2500-2200 for VCE 200 f) 2500-2200 for VCE 550. Note: Panels have different vertical scales.

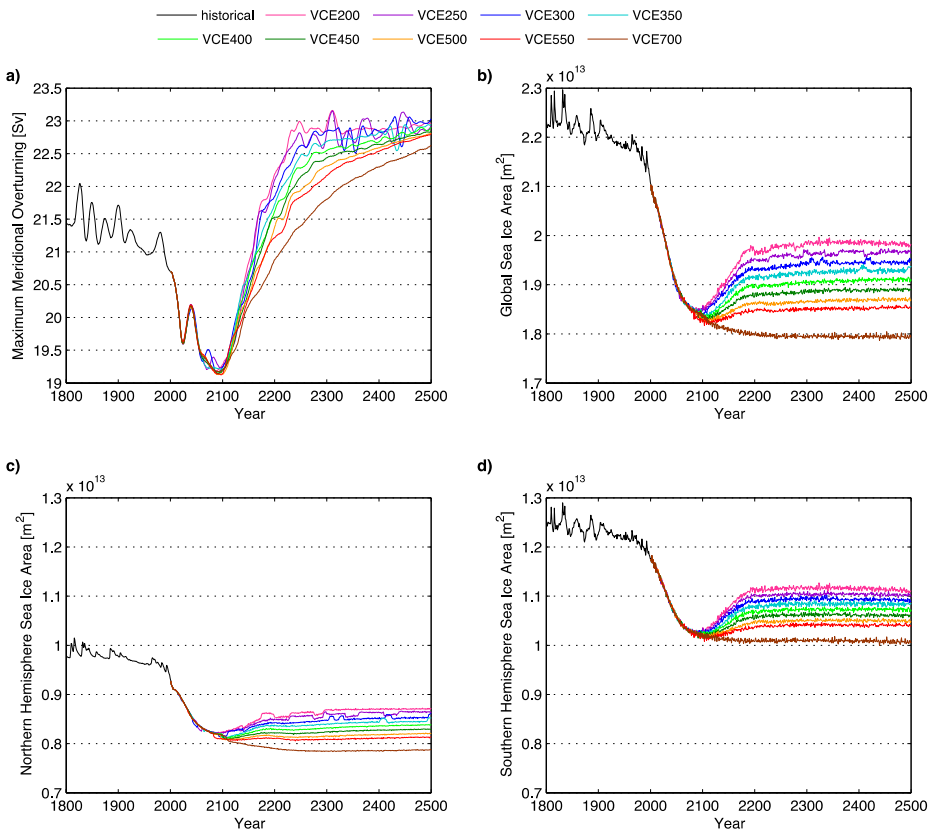

Figure 13. Time series of maximum meridional overturning circulation and sea ice area for VCE simulations (relative to 1801)

Time series of maximum meridional overturning (panel a); global sea ice area (panel b); northern hemisphere sea ice area (panel c); southern hemisphere sea ice area (panel d). Note: The historical values represent the model response to the observed historical forcing.

The maximum overturning circulation (Figure 13 a) reaches its lowest value at 19.1 Sv in year 2089, which is about the same for all VCE pathways. Once the net-negative emissions are implemented, the maximum overturning circulation recovers and the rate of recovery is faster for pathways with larger negative emissions (i.e. faster rate for VCE 200, compared to VCE 550). After cessation of CO_2 emissions, the maximum overturning circulation stabilizes and reaches values of 23.0 Sv and 22.8 Sv, for VCE 200 and VCE 550 respectively, in year 2500.

The global sea ice area (Figure 13 b) decreases more for the VCE 550 pathway compared to VCE 200, until year 2100. Subsequently, it recovers (to different levels for different pathways) and stabilizes in year 2500 at $1.98 \cdot 10^{13}$ m^2 for VCE 200 (11% decline below the pre-industrial level) and $1.85 \cdot 10^{13}$ m^2 for VCE 550 (17% decline below the pre-industrial level).

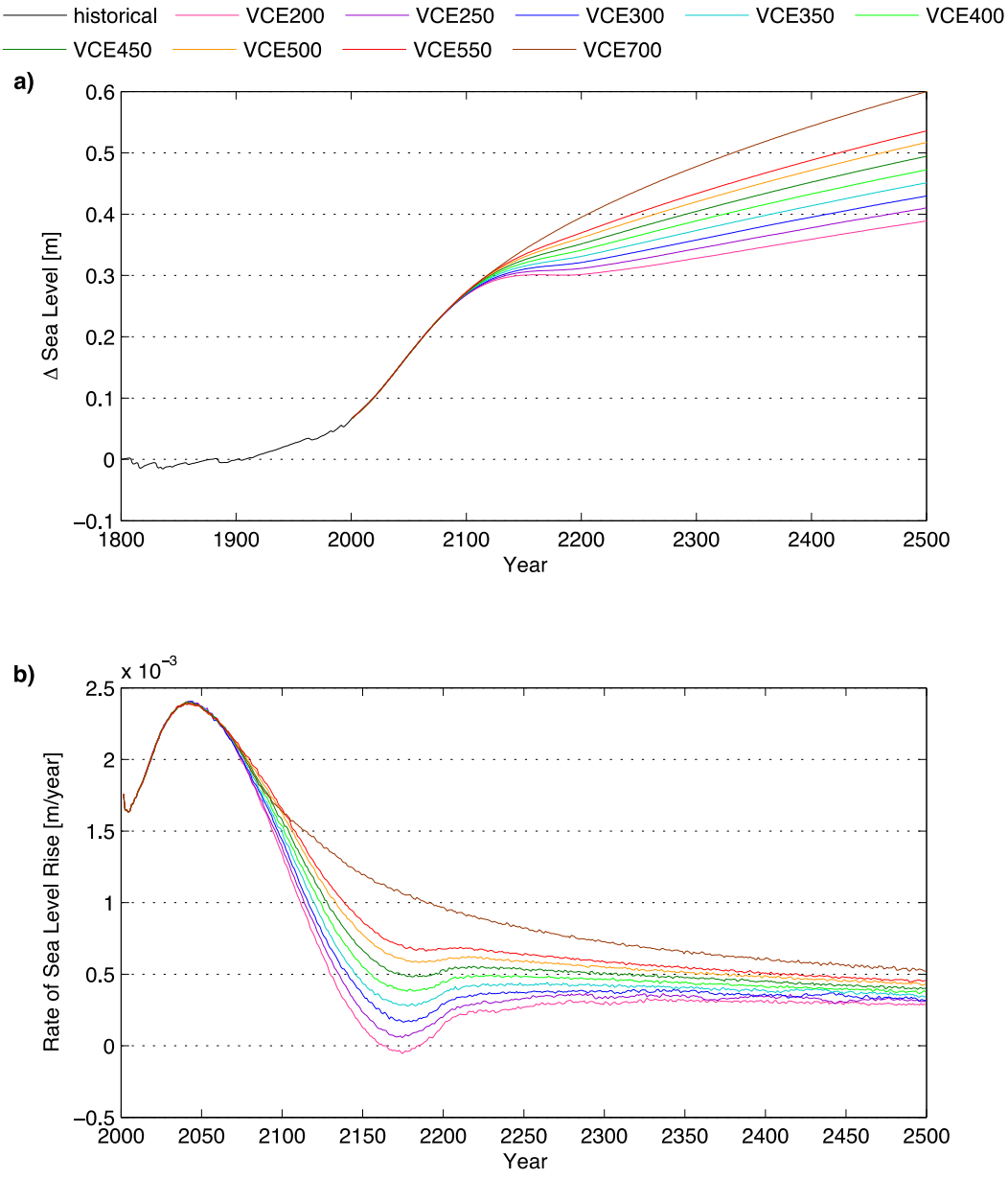

Figure 14. Time series of thermosteric sea level rise and rate of sea level rise for VCE simulations

Time series of relative thermosteric sea level rise with respect to 1801 (panel a) and calculated rate of sea level rise (panel b). Note: The historical values represent the model response to the observed historical forcing.

Despite a large amount of negative emissions implemented in VCE 200, the thermosteric sea level continues to rise (Figure 14 a). The rate of sea level rise after 2070 is lower for VCE 200 compared to VCE 550 (Figure 14 b), which means that larger net-negative emissions are effective in slowing down the rate of the sea level rise, yet not enough to reverse it. However, after the net-negative emissions cease in 2200, the rate of sea level starts to increase again and slowly stabilizes at positive values (ranging from 0.28 to 0.53 cm/year, for different emission pathways). Higher values of the rate of sea level rise are associated with emission pathways entailing greater amounts of cumulative emissions (i.e. VCE 550: 0.46 cm/year; compared to VCE 200: 0.28 cm/year; Figure 14 b).

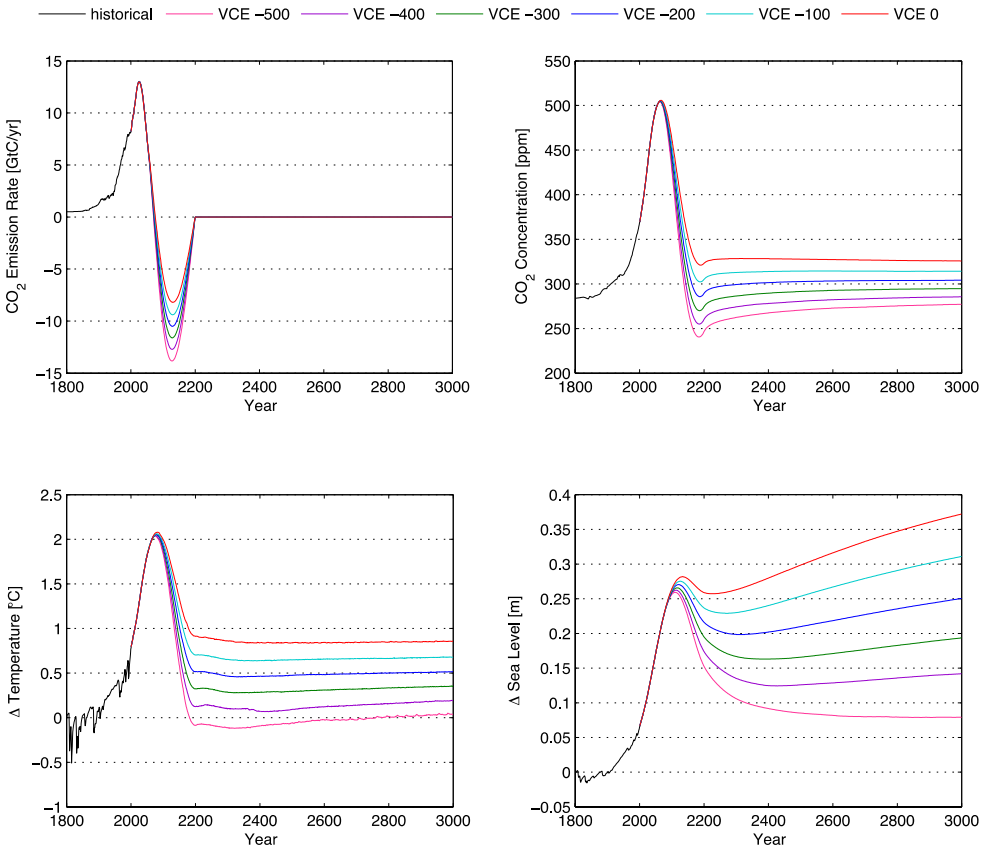

Figure 15. Time series of global variables for VCE_extreme simulations
Time series of CO_2 emission rate (panel a); atmospheric CO_2 concentrations (panel b); global mean surface temperature change relative to 1801 (panel c) and relative sea level rise relative to 1801 (panel b). Note: The historical values represent the model response to the observed historical forcing. Simulation names correspond to cumulative CO_2 emissions since year 2000. The amount of CO_2 artificially removed from the atmosphere during years 2070-2200 to reach the cumulative emission target specified by the pathway name, is given in brackets for each pathway: VCE -500 (1175 GtC); VCE -400 (1077 GtC); VCE -300 (979 GtC); VCE -200 (881 GtC); VCE -100 (784 GtC) and VCE 0 (680 GtC).

Additional simulations were carried out to determine how much net-negative emissions would need to be implemented to reverse the sea level rise and stabilize it. The VCE_extreme emission pathways were designed in a similar fashion to VCE pathways (Figure 15 a), but entail implementations of extremely large amounts of negative emissions, which are beyond technological capabilities currently deemed feasible. The results suggest that only for emission pathway VCE -500, which entails about 1200 GtC removed during the period 2100-2200 and a return of the atmospheric CO_2 concentration below the 1801 level (Figure 15 b), sea level rise is reversed

permanently (Figure 15 d). While the global mean temperature stabilizes at the pre-industrial level after year 2500 (Figure 15 c), the sea level reverses and stabilizes at approximately 0.08 m above the 1801 level for the most extreme VCE -500 emission pathway (Figure 15 d).

While the reversal of sea level is possible with large amounts of negative emissions implemented (1200 GtC), negative emissions of this magnitude are not feasible at the current state of the net-negative emission technology. These findings agree with the research of Bouttes et al. (2013), who showed that sea level is reversible if the CO_2 induced radiative forcing is reduced to pre-industrial values (or even down to -2 W/m^2 below pre-industrial level). Furthermore, if the eustatic sea level rise due to the ice melt were also included in the UVic model, the amount of atmospheric CO_2 required to be artificially removed would be even greater due to the millennial response time scale of ice sheets.

4.1.3. Temperature Response to Cumulative Emissions

The change of instantaneous temperature with respect to cumulative CO_2 emissions is referred to as the Transient Climate Response to cumulative Emissions (TCRE) (Matthews et al., 2009). The TCRE is a measure of the climate response to CO_2 emissions, including both the carbon cycle and the physical climate response (Gillett et al. 2013).

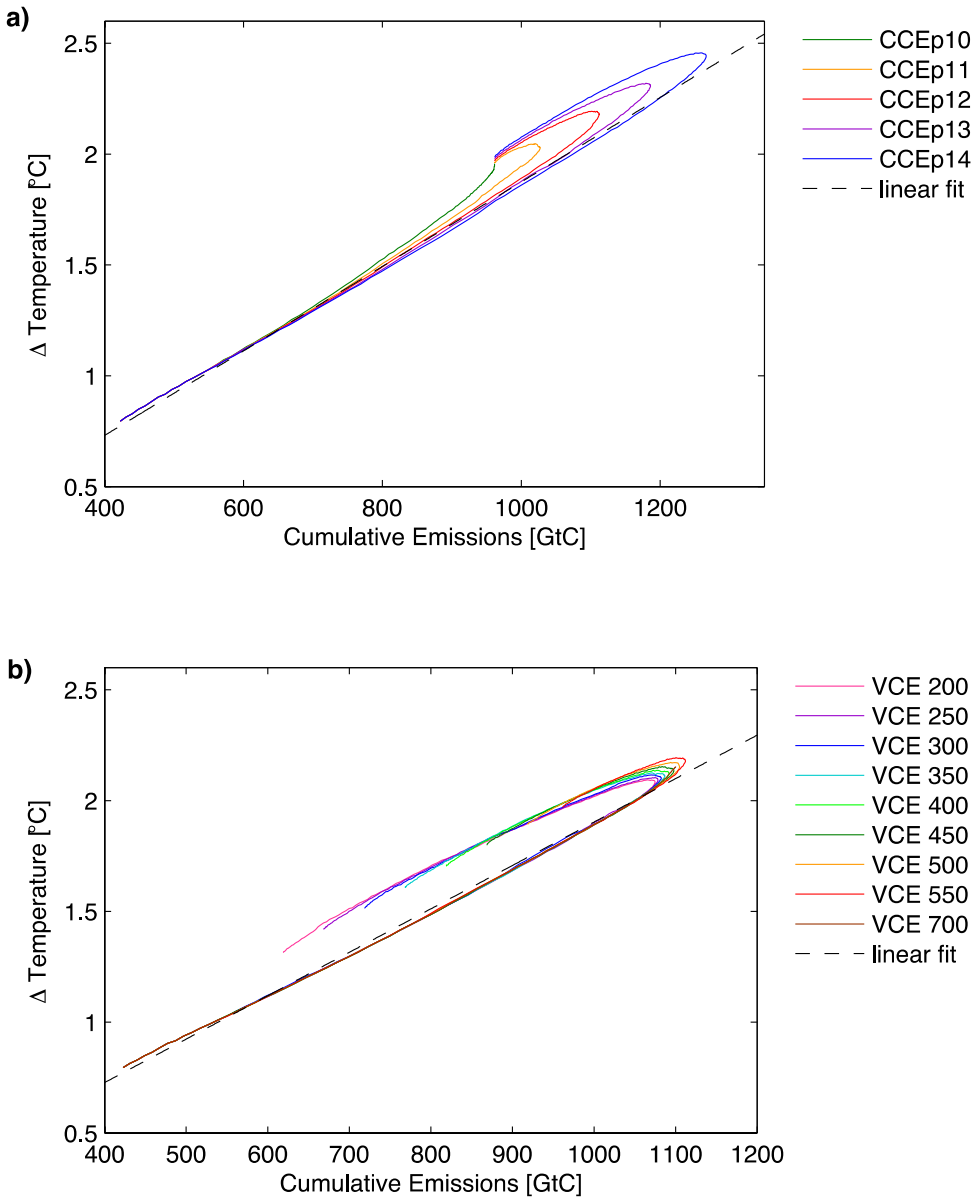

Figure 16. Global mean surface air temperature change as a function of cumulative CO_2 emissions

Temperature (with respect to 1801) as a function of cumulative emissions (with respect to 1801) for CCE simulations (panel a) and for VCE simulations (panel b).

For both simulations (CCE and VCE), the instantaneous temperature response to cumulative emissions shows an approximately linear relation up to the point of maximum

cumulative emissions (around year 2100; Figure 16). The dashed line represents a linear fit to the bottom branch of the TCRE graph, which is calculated using least squares linear regression. In Figure 16 a, the linear fit is shown for the blue pathway (CCEp14), while in Figure 16 b the linear fit corresponds to the red pathway (VCE 550). In both cases, the slope of the linear fit is 2°C per 1000 GtC, which is within the likely range of TCRE values stated by IPCC (2013), i.e. 0.8 to 2.5°C per 1000 GtC. This proportionality of global warming to cumulative emissions is in agreement with studies using other models (Gillett et al., 2013; Matthews et al., 2009; Zickfeld et al., 2012). The linearity results from a combination of two opposite responses: the temperature change per unit of atmospheric CO_2 concentration, which increases at a decreasing rate for higher atmospheric CO_2 levels due to the logarithmic dependence of radiative forcing on CO_2, and the airborne fraction of cumulative emissions, which increases with increasing cumulative emissions (Matthews et al., 2009).

During the positive emissions phase (until year 2100; Figure 16), the simulated temperature values are slightly above the linear fit for lower amounts of cumulative emissions (up to 600 GtC) and slightly below the linear fit for larger amounts of cumulative emissions (between 600 to 1200 GtC). The deviation of the simulated temperature values above the linear fit implies that the increase in radiative forcing per unit change in CO_2 concentrations due to the logarithmic dependence of radiative forcing on atmospheric CO_2 concentrations dominates over the opposing effect of declining airborne fraction at low cumulative CO_2 emissions (Gillett et al., 2013). Conversely, the deviation of the simulated temperature values below the linear fit at higher cumulative CO_2 emissions implies that the saturation in radiative forcing at higher atmospheric CO_2 concentrations dominates over a higher airborne fraction (Gillett et al., 2013; Matthews et al., 2009).

Once net-negative emissions are implemented (years 2100-2200), the temperature curve in Figure 16 turns around and starts to decline, as the cumulative emissions start to decrease due to implementation of net-negative emissions. The temperature decline occurs along a different linear pathway (with similar slope but higher intercept, as compared to the positive emissions phase), showing hysteresis behaviour in temperature. Likely explanations for this hysteresis-like behaviour is a lag in the

responses of climate system components to decreasing cumulative emissions caused by thermal inertia, and the response to non-CO_2 forcings, which are held constant during the model simulations, and do not decline in phase with atmospheric CO_2.

4.2. Carbon Cycle Response

Changes in atmospheric CO_2 are driven by the responses of the marine and terrestrial carbon sinks. The two following sections (4.2.1 and 4.2.2) present a detailed analysis of the terrestrial and marine carbon sinks behaviour during the positive and negative emission phases. Section 4.2.3 summarizes Constant Cumulative Emissions (CCE) and Variable Cumulative Emissions (VCE) simulations results with regard to the carbon cycle responses and quantifies the efficiency of the CO_2 removal from the atmosphere for both sets of simulations.

4.2.1. Changes in Terrestrial Carbon

Changes in the terrestrial carbon reservoir (ΔC_{land}) result from changes in vegetation carbon and soil carbon reservoirs. The two primary fluxes influencing the terrestrial carbon reservoirs are the net primary productivity flux (NPP) and the soil respiration flux, as presented in the schematic diagram (Figure 4) and described in detail in Section 3.2.3.

The following discussion presents a detailed analysis of the terrestrial carbon sink behaviour during the positive and net-negative emission phases for global carbon reservoir changes for both set of scenarios (CCE and VCE), and for the spatial distribution of carbon reservoir changes for two chosen VCE emission pathways: VCE 550, compatible with the 2°C target, and VCE 200, entailing the largest amount of net-negative emissions implemented (456 GtC removed).

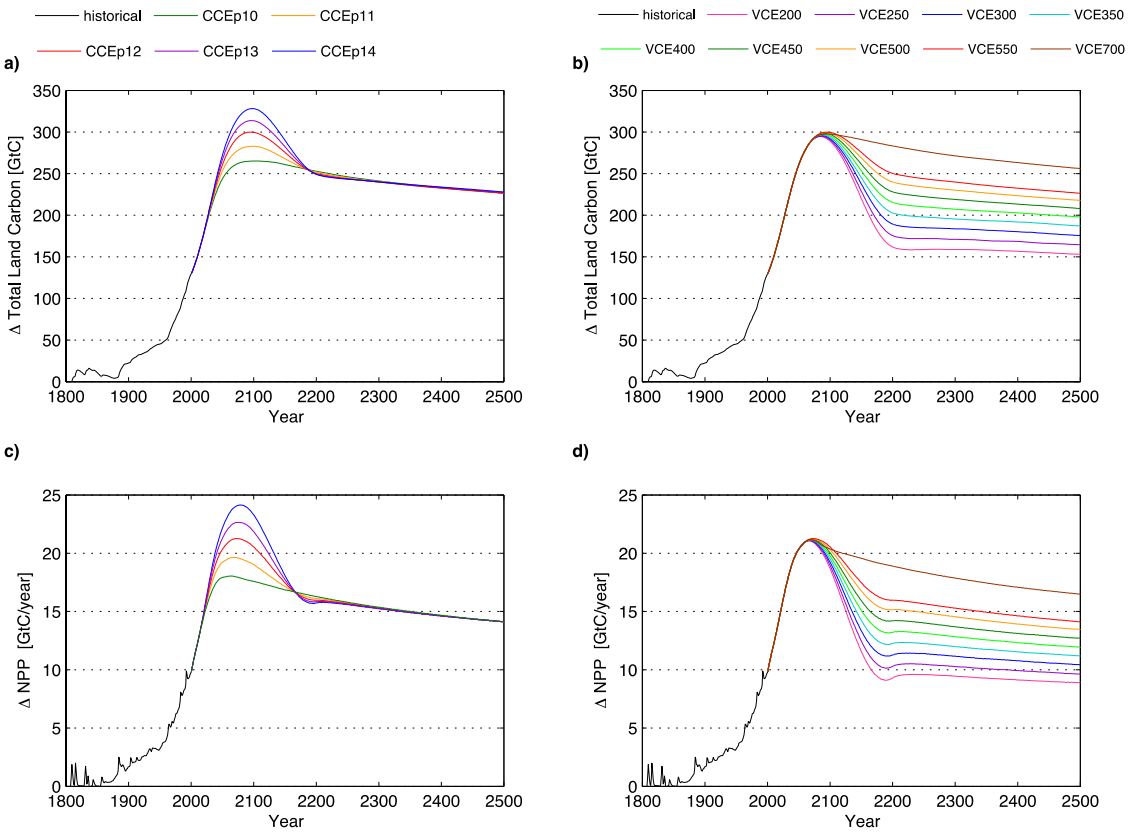

Figure 17. Time series of changes in total land carbon and net primary productivity (NPP) for CCE simulations (left) and VCE simulations (right).

Top panel: time series of changes in total land carbon (left: CCE simulations; right: VCE simulations); bottom panel: changes in NPP (left: CCE simulations; right: VCE simulations); changes are relative to year 1801. Note: The historical values represent the model response to the observed historical forcing.

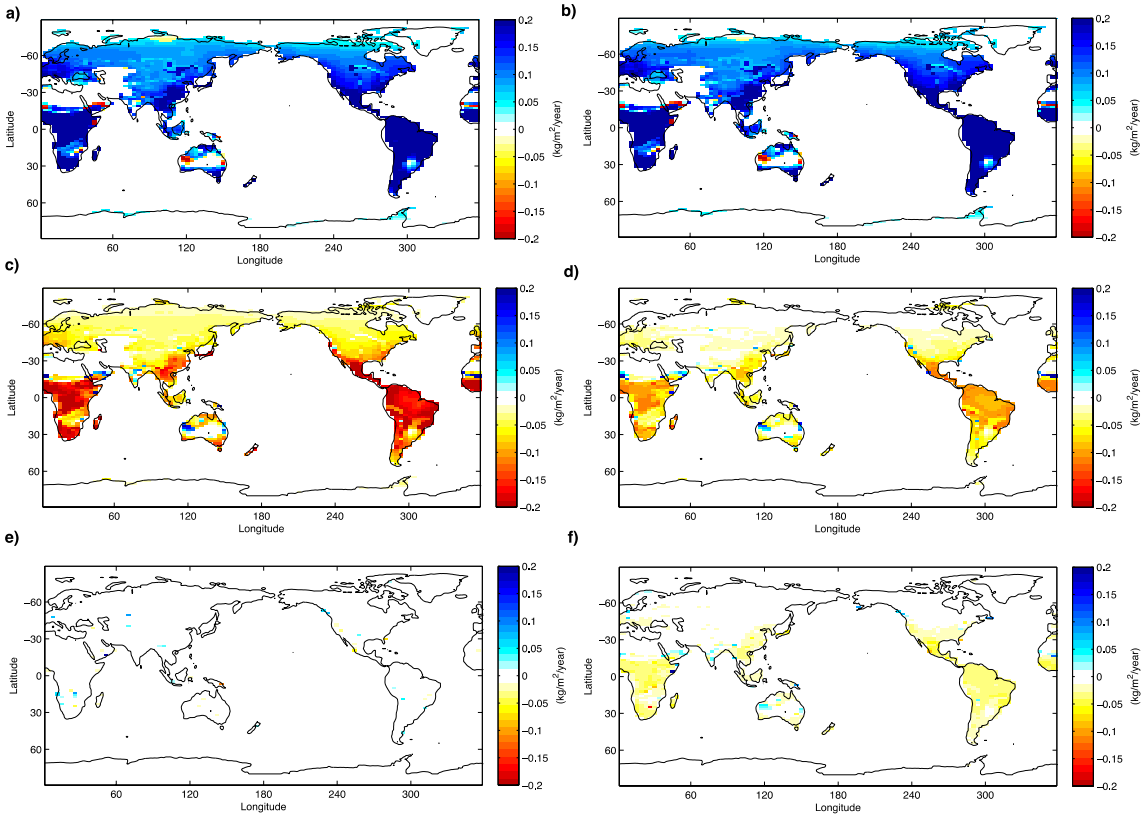

Figure 18. Spatial distribution of net primary productivity for VCE 200 (left) and VCE 550 (right) simulations

Net Primary Productivity distribution for years a) 2100-1810 for VCE 200; b) 2100-1810 for VCE 550; c) 2200-2100 for VCE 200 d) 2200-2100 for VCE 550; e) 2500-2200 for VCE 200 f) 2500-2200 for VCE 550. Note: Red colour indicates outgassing, while blue stands for the carbon uptake.

ΔC_{land} During Positive Emission Phase

During the positive emission phase (until year 2100), the global land carbon continually increases in all simulations (Figure 17 a,b). The increase in global land carbon storage during the positive emission phase (until year 2100) is primarily caused by the CO_2 fertilization effect. Increased atmospheric CO_2 concentration levels enhance photosynthesis, thereby increasing rates of net primary productivity (NPP), leading to an increase in CO_2 uptake by the vegetation. On the other hand, an increase in temperature during the positive emission period leads to an increase in soil respiration rate. Since the loss of CO_2 by soil respiration is smaller than the uptake of CO_2 by vegetation through net-primary productivity (Figure 17 c, d), the global land carbon storage increases during the positive emissions period.

The increase in net-primary productivity is higher for pathways entailing high peak CO_2 emission rates (e.g. CCEp14 compared to CCEp10; Figure 17 c). Although the increase in soil respiration rate is also highest for these pathways, the increase in NPP is greater than the increase in soil respiration. As a result, the global land carbon storage in year 2100 is higher for pathways with higher peak emission rates, as these scenarios entail higher atmospheric CO_2 concentrations and hence a higher CO_2 fertilization effect (Figure 6 a; Figure 17 a).

Spatially, the Tropics and northern mid and high latitudes experience the largest increase in net-primary productivity that leads to an increase in vegetation carbon uptake in those regions (as the increase in NPP is greater than the increase in soil respiration; Figure 18 a,b; Figure 19 a,b). At northern high latitudes, both elevated atmospheric CO_2 concentrations and higher temperature (Figure 12 a,b) promote vegetation growth, as temperature increase at these latitudes brings the temperature closer to the optimal temperature for growth. Warming and elevated atmospheric CO_2 also lead to vegetation shifts, whereby boreal forest and shrub replace C3 grasses (not shown). Increased coverage of boreal forest and shrub at an expense of C3 grass enhances the capacity of vegetation to store carbon, as boreal forest stores more carbon as biomass, compared to C3 grasses.

The main reason for increased carbon storage during the positive emission period (Figure 19 a,b) is the increase in NPP due to elevated CO_2 concentration levels (Figure 18 a,b). The increase in temperature during the positive emissions phase has a negative effect on NPP in the Tropics, as the temperature increases beyond the optimum growth temperature, leading to a decline in NPP. However, this effect is overcompensated by increased atmospheric CO_2 concentration levels and thus, stronger CO_2 fertilization effect, resulting in a net increase in NPP in that region (Figure 18 a,b).

The Tropics also experience an increase in C3 grasses and tropical forest coverage at an expense of shrub. As a result, soil carbon storage increases in that region, as C3 grasses are efficient at carbon cycling and lead to high litter fall, which increases the carbon storage by the soil.

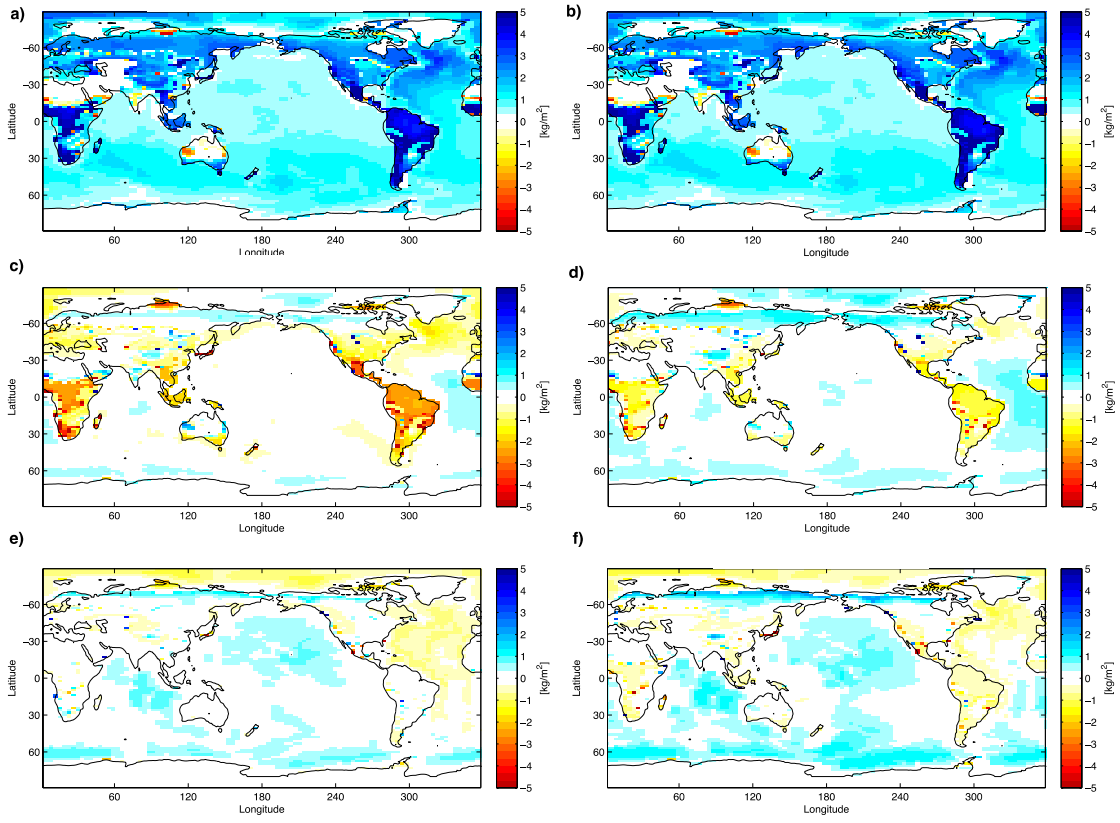

Figure 19. Spatial total carbon distribution for VCE 200 (left) and VCE 550 (right) simulations

Spatial total (land and ocean) carbon storage between years a) 2100-1810 for VCE 200; b) 2100-1810 for VCE 550; c) 2200-2100 for VCE 200 d) 2200-2100 for VCE 550; e) 2500-2200 for VCE 200 f) 2500-2200 for VCE 550. Note: Red colour indicates outgassing, while blue stands for carbon uptake.

ΔC_{land} During the Net-Negative Emission Phase

During the net-negative emissions phase (years 2100-2200), global total land carbon continuously declines for all pathways (Figure 17 a,b). The decline is stronger for pathways entailing larger amounts of negative emissions (e.g. CCEp14, compared to CCEp10; and VCE 200, compared to VCE 550; Figure 17 a,b).

A decline in atmospheric CO_2 concentration levels during this period leads to a decline in net-primary productivity. The decline in NPP is highest for the emission pathways that entail largest amounts of negative emissions (e.g. CCEp14; VCE 200; Figure 17 c,d), as these pathways experienced the largest decline in atmospheric CO_2 concentrations during the net-negative emissions period. Although global soil respiration rate declines as well due to falling temperatures, the decline in global NPP is greater than the decline in soil respiration rate, implying release of CO_2 back to the atmosphere (highest of the pathways CCEp14 and VCE 200).

Spatially, the largest decline in terrestrial carbon storage occurs in the Tropical region (Figure 19 c,d). The leading factor contributing to this terrestrial carbon loss is the decrease in the atmospheric CO_2 concentration and a weakening of the CO_2 fertilization effect. Declining temperature in the Tropics (by approximately 1°C to 1.5°C; Figure 12 c,d) is beneficial for vegetation growth, as the temperature declines closer to the optimum growth temperature. However, this beneficial effect is small compared to the decline in CO_2 fertilization due to lower atmospheric CO_2 levels. Also, the decline in atmospheric CO_2 influences the net-primary productivity rates sooner than the decline in temperature, as the temperature response lags behind the decline in atmospheric CO_2, due to thermal inertia. Soil respiration declines as well, however, the decline in NPP is greater than the decline in soil respiration, leading to outgassing in this region.

An opposite pattern prevails in northern high latitudes, where there is an increase in total land carbon storage during the negative emission phase (Figure 19 c,d), despite a decline in atmospheric CO_2 and temperature in these regions (Figure 12 c,d). The carbon uptake at northern high latitudes (Figure 19 c,d) during the net-negative emission phase occurs due to vegetation shifts, which lag the atmospheric CO_2 and temperature response due to the long (decadal to centennial) timescales of vegetation cover

changes. Boreal forest continues to expand in northern high latitudes at the expense of shrubs, thereby increasing the carbon uptake in that region. The increase in the boreal forest coverage during the net-negative emissions phase is greater for VCE 550, as compared to VCE 200, as a smaller reduction in atmospheric CO_2 and temperature for VCE 550 (Figure 11; Figure 12 c,d) promote the growth of the boreal forest in the northern high latitudes and thus, lead to an increase in the terrestrial carbon storage in that region (Figure 19 c,d). In addition, there is a slight increase in C3 grass coverage in northern high latitudes, which contributes to the land carbon uptake. Globally, however, the carbon uptake in northern high latitudes during the negative emission phase is overcompensated by the total decline in land carbon in the tropics.

ΔC_{land} After Cessation of CO_2 emissions

Once CO_2 emissions reach zero (at 2200), the decline in terrestrial carbon uptake slows down, and land carbon stabilizes between 625 and 661 GtC in year 2500, for pathways VCE 200 and VCE 550, respectively (Figure 17 b). The terrestrial carbon cycle response after emissions are zeroed depends on the cumulative amount of emissions, with land carbon uptake being larger for emission pathways with greater cumulative emissions targets (e.g. VCE 550, compared to VCE 200; Figure 17 b).

For the CCE emission pathways, the long-term terrestrial carbon cycle responses are approximately independent of emission pathway (Figure 17 a,c), as the global terrestrial carbon stabilizes at one level for all pathways, reaching 661 GtC in year 2500.

Spatially, the terrestrial carbon continues to decline slightly in the Tropics and to increase in the northern latitudes (for the period 2200-2500; Figure 19 e,f). Both NPP and soil respiration continue to decline slightly over this period in the Tropics (Figure 18 e,f). Boreal forest coverage continues to expand in the northern high latitudes (thereby leading to higher land carbon storage), while tropical forest continues to decline in the Tropics (thereby leading to lower land carbon storage in that region).

4.2.2. Changes in Ocean Carbon

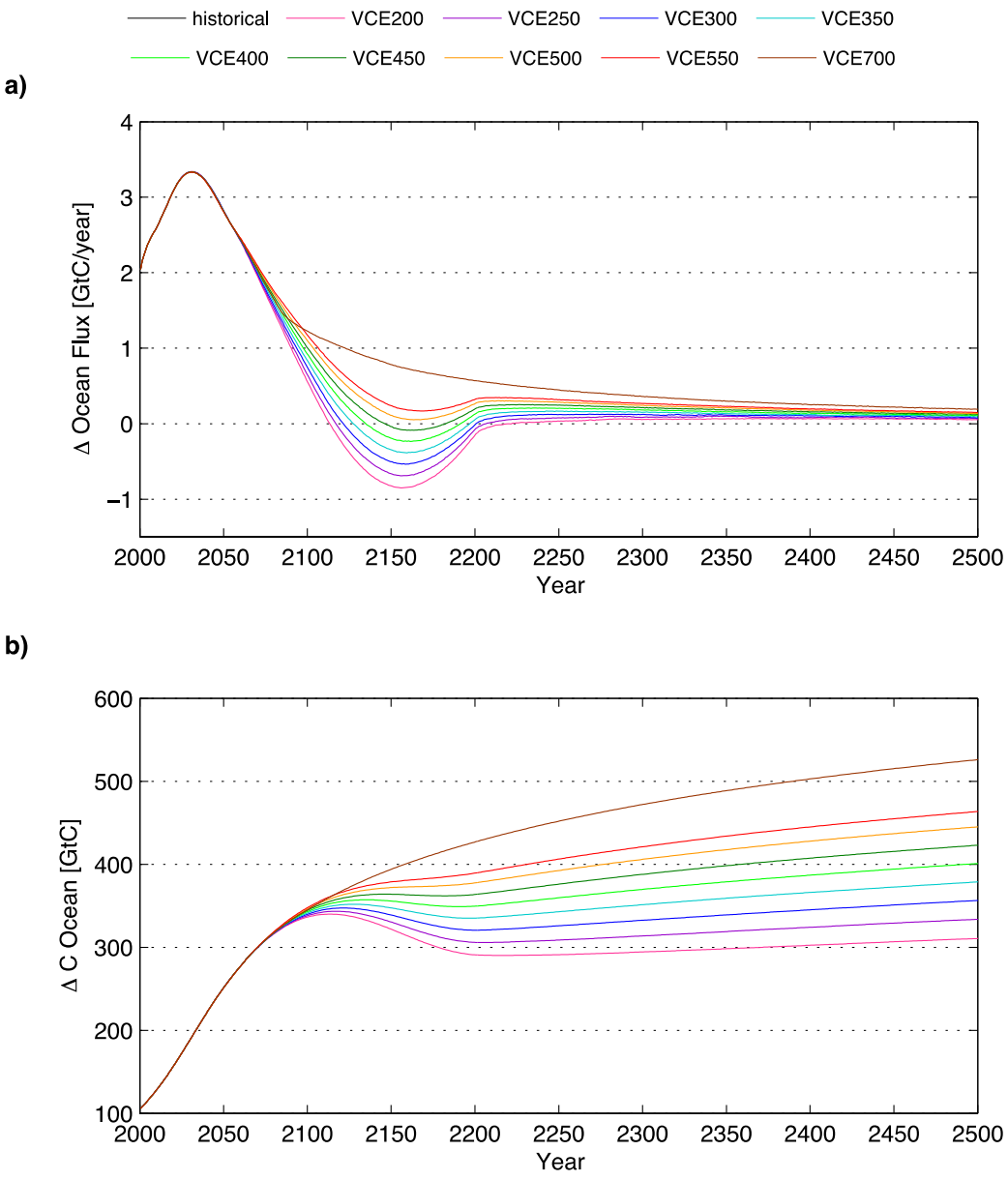

Figure 20. Time series of ocean carbon flux (a) and ocean dissolved inorganic carbon (b) for VCE simulations (changes relative to 1801)

During the positive emissions phase (until year 2100), the atmosphere-ocean flux is positive, indicating that the ocean continually takes up CO_2 from the atmosphere (Figure 20 a). The uptake occurs due to an increase in atmospheric CO_2 concentrations,

which leads to an increase in the CO_2 partial pressure gradient between the ocean surface and the atmosphere, thereby driving a CO_2 flux into the ocean.

Increasing global mean temperature during the positive emissions period leads to warmer surface ocean temperature, which decreases the solubility of CO_2 in ocean waters, thereby slowing down carbon uptake by the ocean. Furthermore, warming of the ocean surface waters and freshening of the high latitude ocean due to increased precipitation over evaporation and ice melt lead to increased stratification and a slow down of the meridional overturning circulation (Section 4.1.2). However, these negative effects of temperature on ocean carbon uptake do not outweigh the positive effects of elevated atmospheric CO_2, so that the ocean is a net sink of CO_2.

The changes in the ocean carbon flux impact the ocean carbon reservoir: if the atmosphere-ocean flux is positive (toward the ocean), the ocean carbon storage increases (Figure 20 b). Atmospheric CO_2 is absorbed and dissolved in the surface ocean waters in a form of dissolved inorganic carbon (DIC; of approximate pool size 38,000 GtC), which consists of three components: carbonic acid (CO_2 dissolved in water), bicarbonate [HCO_3^-] and carbonate ions [CO_3^{2-}] (Denman, 2008; IPCC, 2013). Marine biota (primarily phytoplankton) constitutes additional 3 GtC of organic ocean carbon content (IPCC, 2013). Due to the relatively small size of the organic ocean carbon, changes in this pool are neglected, and changes in DIC are in the following assumed to be equal to changes in total ocean carbon storage.

The increase in carbon storage during the positive emission phase is rapid at the surface and slower at deeper levels, as a result of the centennial timescale of deep-ocean mixing between the surface waters and intermediate and deep ocean waters.

Spatially, during the positive emission phase (until year 2100) the atmosphere-ocean flux is positive in most regions, except for strong outgassing in the equatorial Pacific (Figure 21 a,b). The uptake is strongest in the tropical oceans (particularly the Tropical Pacific), the North Atlantic and the Southern Ocean. In the Tropical Pacific (both north and south of the Equator), warmer surface waters enhance biological productivity, resulting in greater transport of carbon to deeper ocean layers, thereby increasing the capacity of carbon uptake (Zickfeld et al., 2011). Furthermore, warm temperatures

promote faster remineralisation of organic matter and formation of DIC in subsurface waters, which are brought up to the surface by upwelling in the Equatorial Pacific, leading to CO_2 outgassing in that region (Zickfeld et al., 2011). In the North Atlantic, strong carbon uptake occurs due to deep-water formation, which leads to mixing of deep waters with surface waters. The transport of carbon from the surface down to deep waters enhances the capacity of surface waters to capture more atmospheric carbon. As a result of the dominantly positive (downward) CO_2 flux, ocean dissolved inorganic carbon (DIC) increases during the positive emission period in all regions of the ocean (Figure 19 a,b).

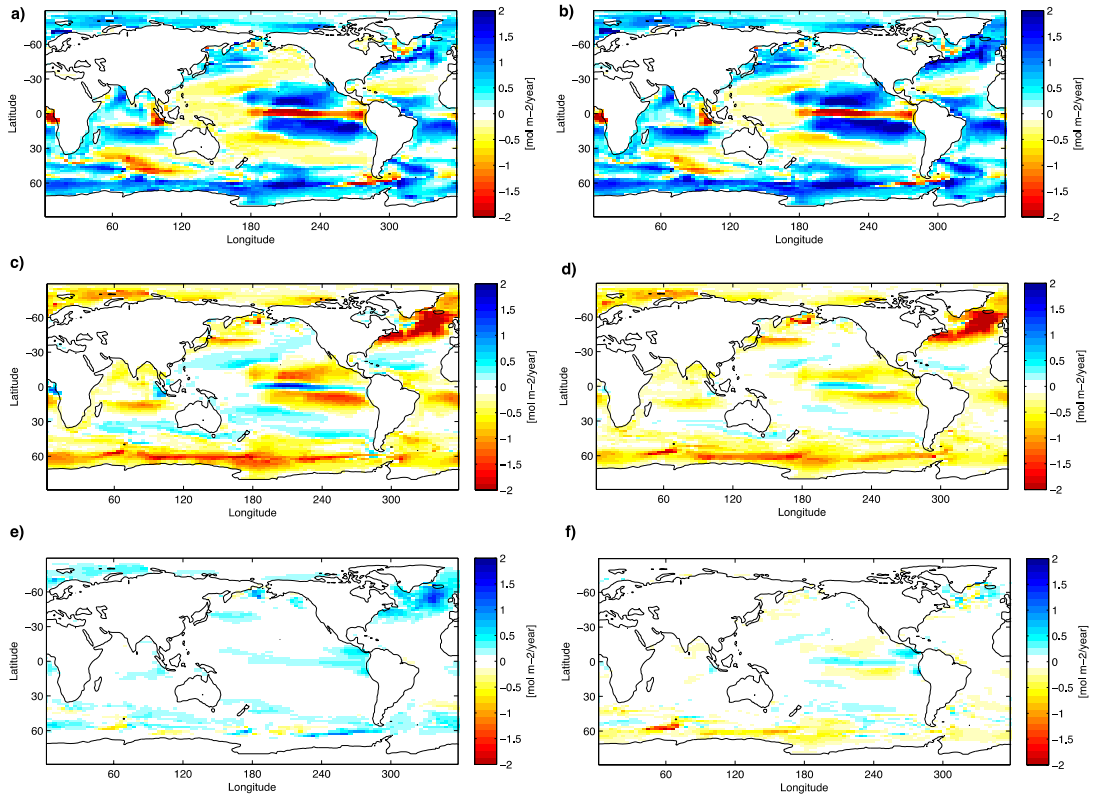

Figure 21. Ocean flux distribution for VCE 200 (left) and VCE 550 (right) simulations

Spatial changes in ocean flux distribution between years: a) 2100-1810 for VCE 200; b) 2100-1810 for VCE 550; c) 2200-2100 for VCE 200 d) 2200-2100 for VCE 550; e) 2500-2200 for VCE 200 f) 2500-2200 for VCE 550. Note: Red colour signifies outgassing, while blue stands for the carbon uptake.

The implementation of negative emissions during the period 2100-2200 causes a decrease in atmospheric CO_2 concentration levels, leading to a decrease in the CO_2

partial pressure between the ocean and the atmosphere. For pathways that entail large amounts of negative emissions (e.g. VCE 200), the decrease in partial pressure is large enough to change the direction of the CO_2 flux and drive it away from the ocean (Figure 20a). For pathways with a small amount of negative emissions implemented (e.g. VCE 550; Figure 20 a), the flux remains positive (towards the ocean) but is much weaker than during the positive emissions phase. Correspondingly, ocean carbon storage also decreases during this period for pathways that entail large amounts of negative emissions (Figure 20 b).

Spatially, during the net-negative emissions period, the outgassing occurs mostly in the Southern Ocean, North Atlantic and tropical Pacific (Figure 21 c,d), i.e. the regions with the strongest CO_2 uptake during the positive emission phase. The pattern of outgassing is consistent with that found in a study that used a complex Earth system model (CMCC-CESM) (Vichi et al., 2013).

After year 2200, once emissions are zeroed, the ocean CO_2 flux stabilizes for all pathways at a positive value (toward the ocean; reaching 0.2 GtC/year in year 2500; Figure 20 a). Thus, the ocean continues to take up atmospheric CO_2 beyond the year 2500 (Figure 19 e,f; Figure 20 a). At year 2500, cumulative ocean carbon uptake ranges from 311 to 526 GtC (Figure 20 a).

4.2.3. Efficiency of the CO_2 removal

Our results from the analysis of the carbon cycle variables show that the efforts to artificially remove CO_2 from the atmosphere during the net-negative emissions period (years 2100-2200) are offset by outgassing of CO_2 from the natural carbon sinks. The larger the amount of net-negative emissions implemented (largest in the VCE 200 simulation), stronger the outgassing from both the ocean and terrestrial biosphere.

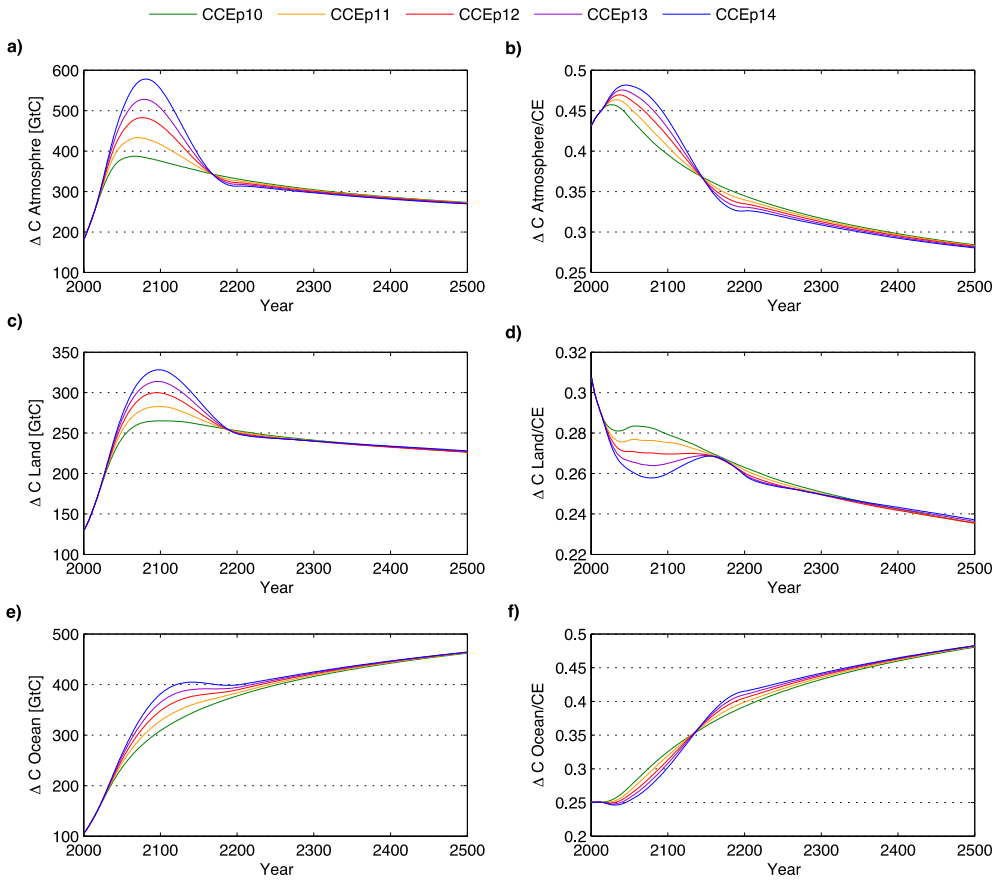

Figure 22. Time series of global carbon cycle variables for CCE simulations
Time series of atmospheric carbon burden change since 1801 (panel a); atmospheric carbon burden change as a fraction of cumulative emissions (CE) (airborne fraction) (panel b); change in total land carbon since 1801 (including vegetation and soil carbon) (panel c); land uptake fraction (panel d); change in ocean carbon since 1801 (panel f); Ocean uptake fraction. Note: Panels have different vertical scales.

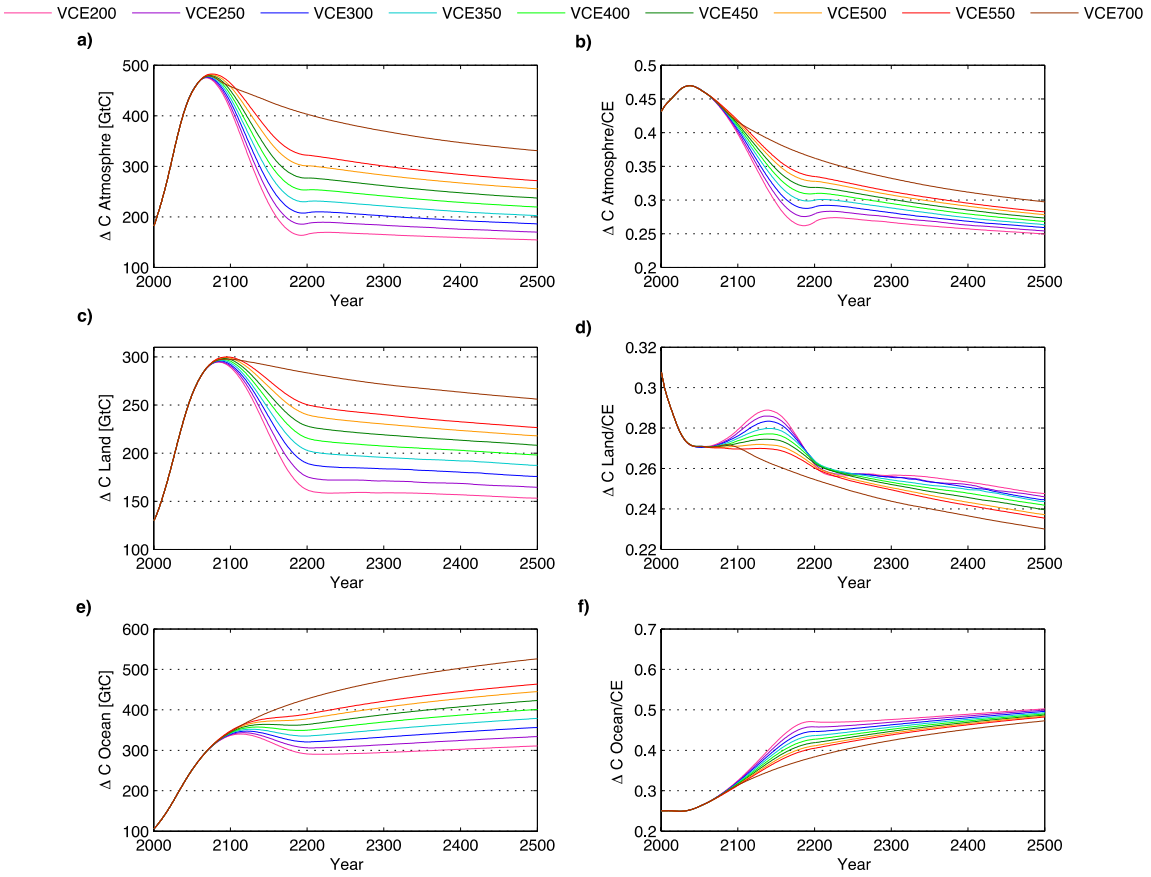

Figure 23. Time series of global carbon cycle variables for VCE simulations
Time series of atmospheric carbon burden change since 1801 (panel a); atmospheric carbon burden change as a fraction of cumulative emissions (CE) (airborne fraction) (panel b); change in total land carbon since 1801 (including vegetation and soil carbon) (panel c); land uptake fraction (panel d); change in ocean carbon since 1801 (panel f); Ocean uptake fraction. Note: Panels have different vertical scales.

To quantify the effectiveness of the net-negative emissions, we define an efficiency measure as the ratio of the change in atmospheric CO_2 burden to cumulative CO_2 emissions (Figure 22; Figure 23). This measure is commonly referred to as the airborne fraction of cumulative emissions.

During the positive emissions phase (until year 2100), the airborne fraction (shown in Figure 22 b and Figure 23 b for CCE and VCE pathways, respectively), increases, peaks around year 2050, followed by a continuous decline. The highest increase in the airborne fraction occurs for pathway CCEp14 (Figure 22 b), which entails the highest peak emission rate (14 GtC/yr) and the largest amount of cumulative emissions emitted during the positive emissions phase (until year 2100). After the peak, the decline in airborne fraction is steeper for pathways with higher peak emission rates.

During the net-negative emissions period in years 2100-2200, the efficiency measure can be understood as the drop in atmospheric CO_2 per unit (negative) cumulative emissions removed (Figure 22 b; Figure 23 b). The higher the drop in atmospheric CO_2 per unit of cumulative emissions is, the more efficient the implementation of net-negative emissions. Our results show that the larger the amount of negative emissions, the lower the efficiency of artificial CO_2 removal, meaning a smaller drop in atmospheric CO_2 per unit of cumulative emissions. Figure 22 b and Figure 23 b show that the drop in atmospheric CO_2 per unit cumulative emissions is lowest for the pathways that entail largest amounts of net-negative emissions implemented (CCEp14 and VCE 200, respectively).

Once emissions are zeroed (after year 2200), the airborne fraction stabilizes at different levels for different emissions pathways from the VCE experiments (Figure 23), where the lowest efficiency value occurs for the emission pathway VCE 200, which entails the largest amount of negative emissions implemented. For the CCE experiments, the terrestrial and marine uptake fractions, as well as the airborne fraction (Figure 22) converge to the same values after cessation of emissions. Therefore, the long-term efficiency of carbon removal in the CCE simulations is independent of the emission pathway, and only depends on the cumulative emission target.

Chapter 5. Discussion

5.1. Model-based Uncertainties

The value of the equilibrium climate sensitivity is one of the major uncertainties in this research. Equilibrium climate sensitivity is defined as the global mean temperature at which the climate system stabilizes for doubling of the atmospheric CO_2 concentration (IPCC, 2007). The best estimate for the value of the climate sensitivity is 3˚C, and its value is likely (probability > 66%) in the range 1.5-4.5˚C (IPCC, 2013). In the UVic model, the equilibrium climate sensitivity can be altered by including an adjustable feedback between temperature and outgoing long-wave radiation (Zickfeld et al., 2009). Such a parameterization allows to dampen or enhance the increase in outgoing long-wave radiation as temperature rises. As a result, the equilibrium temperature response to doubling of the atmospheric CO_2 level can be different than the standard equilibrium climate sensitivity of the UVic ESCM of 3.5°C. Choosing higher values of equilibrium climate sensitivity would make the model results more responsive to radiative forcing, thereby leading to stronger warming. As a result, the amount of net-negative emissions needed to reverse the temperature to a given level would need to be greater. Also, larger climate sensitivity values leading to stronger warming would make the sea level rise even more difficult to slow down. To account for the uncertainties related to the value of the equilibrium climate sensitivity, each of the simulations could be run for a range of climate sensitivity values (e.g. from 1.5-4.5˚C), to explore how the value of climate sensitivity influences the model outputs. However, this approach would require additional time and computing power to run each simulation multiple times.

Another uncertainty is related to the future evolution of the radiative forcing from non-CO_2 greenhouse gases and aerosols. Since the future emission pathways for these gases are highly uncertain, the forcing was held fixed at year-2010 values for future years. Currently, the forcing from other greenhouse gases approximately cancels out the

effects of sulphate aerosols, thus, fixing both forcings at the year-2010 values, assumes that this offsetting effect will continue into the future. However, the aerosol forcing may decrease in the future (IPCC, 2007), and in such case the actual warming would be more severe than shown by this model. On the other hand, setting the future forcing from other greenhouse gases, sulphate aerosols to constant values allow us to focus on the CO_2 from fossil fuel emissions as the main forcing in the climate system. An alternative approach is to make assumptions about the future pathways for other greenhouse gases and sulphate aerosols. Inclusion of other non-CO_2 gases may not have much impact on changes in reversibility of the climate system, since these gases are short-lived, as compared to CO_2.

The UVic model slightly overestimates the thermosteric sea level rise over the historical period compared to observations, due to an overestimate of the ocean heat uptake (Eby et al., 2009). This likely implies an overestimation of the thermosteric sea level rise component in future simulations as well. However, the 2.9 version of the UVic ESCM does not include a dynamic ice sheet model, thereby largely underestimating the total (thermosteric and eustatic) future sea level rise. IPCC (2013) estimates the eustatic sea level rise to range from 0.12 to 0.26 m by the year 2100 for the high emission scenario RCP 8.5 and from 0.07 to 0.17 m for the low emission scenario RCP 2.7 (IPCC, 2013). However, the projections of ice sheet contribution to sea level rise are highly uncertain, making it difficult to determine an upper bound for the eustatic sea level rise (IPCC, 2013). Accounting for the eustatic sea level rise would cause even larger total sea level rise, requiring greater amounts of negative emissions in order to slow it down. The reversibility of sea level rise could also be affected, as sea level rise from the ice melt will be difficult to reverse due to the long response timescale of ice sheets.

The carbon permafrost feedback is not included in the 2.9 version of the UVic model either, which could create additional sources of irreversibility on centennial timescales (Zickfeld et al. 2013). Including the permafrost feedback in the model would slow down the decline in atmospheric CO_2 and global mean temperature, as greenhouse gases, such as methane, are released from the permafrost and contribute to climate warming. As a result, an even greater amount of net-negative emissions would need to be implemented to offset the temperature increase caused by greenhouse gases

released from the melted permafrost. Natural restoration of permafrost occurs on centennial to millennial timescales (MacDougall et al., 2012), which could impact the timescales of reversibility of climate system components.

In addition, to verify the robustness of the model results, the emission pathways designed for the purpose of this study could be an input to a more complex Earth system model, which would include more processes and feedbacks (e.g. dynamic ice-sheet model and permafrost feedbacks).

5.2. Risks Related to the Implementation of Negative Emissions Technologies

Krey and Riahi (2009) emphasized that the main advantage of net-negative emissions (mostly in the form of bioCCS) is the ability to influence the timing of mitigation and postponing the action to the future, in addition to reducing the overall costs of mitigation (Krey & Riahi, 2009). Without net-negative CO_2 capture, earlier action is needed to reduce CO_2 emissions to near zero-levels (Krey, & Riahi, 2009).

While negative emission technologies provide the ability to influence the timing of mitigation (Krey & Riahi, 2009), they create a moral hazard, as they give an opportunity for policy makers to postpone their actions now and use those technologies more aggressively later, to achieve the same cumulative CO_2 emission targets (Clarke et al., 2009). Despite the ability to capture excess atmospheric CO_2, a transition to a lower carbon energy system is still required (Ranjan, & Herzog, 2011), as it would be more cost effective to limit emissions in the first place.

Using the unit cost estimates of implementation of negative emission technologies (based on a full-life cycle analysis and presented in Section 2.3.2), we calculated the approximate cost of implementing direct air capture and bioCCS for three chosen emission pathways (CCEp14, CCEp12 that is equivalent to VCE 550, and VCE 200). As indicated in Table 4, the cost of implementation of negative emissions at the scale assumed in this study is very high. It should be noted that the risks of such implementation (e.g. accounting for leakage of CO_2 from geological formations or food

supply chain conflicts, in case of bioCCS) are not included in the cost estimates (Section 2.3; McGlashan et al., 2012).

Table 4. Sample cost estimates of implementing negative emissions

Emission Pathway	Negative Emissions Implemented [GtC]	Direct Air Capture Estimated Cost [trillion $]	BioCCS Estimated Cost [low-high] Range [trillion $]
CCEp12 (equivalent to VCE 550)	-151	85.9	32.6-61.5
CCEp14	-305	173.5	66.0-124.2
VCE 200	-456	259.4	98.7-185.8

Note: The cost estimates are based on a full-life cycle analysis of negative emission technologies (McGlashan et al., 2012) and do not consider future discount rate. Conversion factor used: 1GtC =3.67 Gt CO_2. The present value of these costs would be higher, if a positive future discount rate was considered.

Chapter 6. Conclusions

6.1. Summary of the Main Results

This research analyses the responses of the climate system components to custom-designed CO_2 emission pathways that meet feasibility constraints of net-negative emission technologies. The pathways follow a gradual transition from the current, fossil fuel driven economy, to a zero-emission energy system. The fossil fuel emissions peak within the next few decades (2018-2030) and decline to zero by year 2100 at a maximum rate of 6%. This period of declining emissions is followed by implementation of negative emissions during 2100-2200. We performed two sets of simulations: constant cumulative emissions simulations (CCE; where the pathways vary in peak and negative emission rates but entail the same net cumulative emissions by year 2500, 550 GtC) and variable cumulative emissions simulations (VCE; where the cumulative amount of emissions ranges between 200-700 GtC for different pathways).

Our results show that during the positive emission phase (until year 2100) the global mean temperature increases, by up to 2.5°C above pre-industrial for the pathway with the highest peak emission rate (CCEp14). Temperature increases in all regions, with the largest warming in the northern high latitudes. Consequently, the area of sea ice declines (up to 20% decline of the pre-industrial coverage), the meridional overturning circulation slows down and the sea level continually rises (by up to 0.3 m) during this period.

Net-negative emissions in our experiments (ranging from 66 GtC to 456 GtC removed) decrease the amount of atmospheric CO_2 and lead to lower atmospheric CO_2 concentration levels. The atmospheric CO_2 decline is sufficient to reverse the global mean temperature and to stabilize it at a desired level (2°C above the pre-industrial temperature in year 2200). Also, changes in the meridional overturning circulation and sea ice are reversible with the artificial removal of CO_2 from the atmosphere.

However, despite large amounts of net-negative emissions implemented (up to 456 GtC removed), thermosteric sea level continues to rise and is not reversible on human timescales. While negative emissions are able to decrease the rate of sea level rise, soon after their cessation (in year 2200) the rate of sea level rise increases again. Stabilization of sea level at a desired (low) value would require a continuous artificial removal of the atmospheric CO_2 in order to offset the delayed warming resulting from the thermal inertia of the ocean. Reductions in atmospheric CO_2 required for the sea level to decline (approximately 1200 GtC removed) are far beyond current capabilities of negative emissions technology.

During the period of positive emissions (until year 2100), both the ocean and the terrestrial biosphere act as carbon sinks, taking up CO_2 from the atmosphere through the CO_2 fertilization effect on land and the increase in the CO_2 partial pressure between the ocean and the atmosphere which drives a CO_2 flux into the ocean.

During the net-negative emission period (years 2100-2200), artificial removal of the atmospheric CO_2 leads to lower atmospheric CO_2 concentration levels. On land, declining atmospheric CO_2 concentrations weaken the CO_2 fertilization effect, leading to a decline in net-primary productivity and result in outgassing of CO_2 from the terrestrial carbon sink. In the ocean, declining atmospheric CO_2 concentrations also lead to a decrease the partial pressure between atmosphere and the ocean, leading to a decline in the ocean carbon storage. For emission pathways that entail large amounts of negative emissions (e.g. VCE 200), the decrease in the partial pressure is significant enough to change the atmosphere-ocean flux direction, resulting in the ocean acting as a carbon source and releasing CO_2 back to the atmosphere. The largest decline in terrestrial carbon storage occurs in the Tropical region, which is partially compensated by atmospheric CO_2 uptake by the northern high latitudes. In the ocean, outgassing occurs mostly in the Southern Ocean, North Atlantic and tropical Pacific.

During the net-negative emission phase, the release of CO_2 from the natural (terrestrial and marine) carbon sinks reduces the effectiveness of atmospheric CO_2 removal, here defined as the change in atmospheric CO_2 burden to cumulative CO_2 emissions. The largest outgassing occurs for pathways entailing largest amounts of net-

negative emissions implemented (e.g. VCE 200; CCEp14), implying that the efficiency of net-negative emissions decreases the most for these pathways.

6.2. Significance of Results and Implications

Previous studies have predominantly focused on exploring the temperature response under zero-emission scenarios, which entail complete cessation of CO_2 emissions at a given year. A few studies that included net-negative emission pathways (e.g. Boucher et al., 2012; MacDougall, 2013) assume unrealistically high rates of negative emissions. On the contrary, our study used plausible emission pathways, where negative technologies are implemented at technologically feasible rates.

Furthermore, we have explored responses of various Earth system components on global and regional scales. Our study provides a detailed analysis of terrestrial and marine carbon sinks responses to a gradual implementation of negative emissions, which has not been discussed in other studies. While Cao and Caldeira (2010) provide discussion of carbon sinks responses, their emission scenarios are highly idealized and entail only extreme one-time CO_2 removal. The research of Vichi et al. (2013) focuses only on the ocean carbon cycle responses and does not include analysis of the terrestrial carbon cycle.

These findings may be of interest to policy makers, as the possibility of the implementation of net-negative technologies in the future would require slower transition to a zero-emission energy system, while still stabilizing the temperature at a desired level (2°C above the pre-industrial level). As mentioned by Kriegler et al. (2012), the advantage of using net-negative technologies is “the ability to decouple emissions and emission control in time and space” (p.2), which would allow for using carbon-intensive fossil fuels for the next few decades (Kriegler et al., 2012).

The key finding of our research, a decline in efficiency of net-negative emissions due to outgassing of natural carbon sinks shows that implementation of negative emission technologies needs to be carefully analyzed in conjunction with terrestrial and marine carbon sinks responses. Our research showed that while it is possible to revert

the global mean temperature to the 2˚C level above the pre-industrial temperature, other components of the climate system are not easily reversible. The amount of net-negative emissions required for sea level to reverse and stabilize at desired levels is large (up to 1175 GtC removed) and may be well beyond technological capabilities of negative emission technologies.

Therefore, while net-negative emissions may be an option during a slow transition to a zero-emission energy system, they should not be used as an excuse for postponing climate change mitigation actions. Consequently, our results suggest that the world's efforts should focus on mitigation now, rather than relying on future technologies which large-scale applicability still needs to be proven.

References

Allen, M. R., & Ingram, W. J. (2002). Constraints on future changes in climate and the hydrologic cycle. Nature, 419(6903), 224-232. Retrieved from http://dx.doi.org.proxy.lib.sfu.ca/10.1038/nature01092

Archer, D., Eby, M., Brovkin, V., Ridgwell, A., Cao, L., Mikolajewicz, U., … Tokos, K. (2009). Atmospheric lifetime of fossil fuel carbon dioxide. Annual Review of Earth and Planetary Sciences, 37(1), 117-134. doi: 10.1146/annurev.earth.031208.100206

Archer, D., Kheshgi, H., & Maier-Reimer, E. (1997). Multiple timescales for neutralization of fossil fuel CO_2. Geophysical Research Letters, 24(4), 405-408. doi: 10.1029/97GL00168

Arora, V. K., Boer, G. J., Friedlingstein, P., Eby, M., Jones, C. D., Christian, J. R., … Wu, T. (2013). Carbon-Concentration and Carbon-Climate feedbacks in CMIP5 earth system models. Journal of Climate, 26(15), 5289-5314. doi:10.1175/JCLI-D-12-00494.1

Azar, C., Lindgren, K., Obersteiner, M., Riahi, K., Vuuren, D., Elzen, K. M. J., … Larson, E.(2010). The feasibility of low CO_2 concentration targets and the role of bio-energy with carbon capture and storage (BECCS). Climatic Change, 100(1), 195-202. doi: 10.1007/s10584-010-9832-7

Boucher, O., Halloran, P.R., Burke, E.J., Doutriaux-Boucher, M., Jones, C.D., Lowe, J., … Wu,P. (2012). Reversibility in an earth system model in response to CO_2 concentration changes. Environmental Research Letters, 7(2), 024013. Retrieved from http://stacks.iop.org.proxy.lib.sfu.ca/1748-9326/7/i=2/a=024013

Bouttes, N., Gregory, J. M., & Lowe, J. A. (2013). The Reversibility of Sea Level Rise. Journal of Climate, 26, 2502-2513.

Brovkin, V., Petoukhov, V., Claussen, M., Bauer, E., Archer, D., & Jaeger, C. (2009). Geoengineering climate by stratospheric sulfur injections: Earth system vulnerability to technological failure. Climatic Change, 92(3-4), 243-259. doi: 10.1007/s10584-008-9490-1

Calvin, K., Edmonds, J., Bond-Lamberty, B., Clarke, L., Kim, S. H., Kyle, P., … Wise, M. (2009). 2.6: Limiting climate change to 450 ppm CO_2 equivalent in the 21st century. Energy Economics; International, U.S. and E.U. Climate Change Control Scenarios: Results from EMF 22, 31, Supplement 2(0), S107-S120. Retrieved from http://www.sciencedirect.com.proxy.lib.sfu.ca/science/article/pii/S0140988309001029

Cao, C., & Caldeira, K. (2010). Atmospheric carbon dioxide removal: long-term consequences and commitment. Environmental Research Letters, 5, 024011.

Ciais, P., Sabine, C., Bala, G., Bopp, L., Brovkin, V., Canadell, J., … Thornton, P. (2013). Carbon and Other Biogeochemical Cycles. In: Climate Change 2013: The Physical Science Basis. Contribution of Working Group I to the Fifth Assessment Report of the Intergovernmental Panel on Climate Change [Stocker, T.F., Qin, D., Plattner, G.-K., Tignor, M., Allen, S.K., Boschung, J.,… Midgley, P.M.]. Cambridge University Press, Cambridge,United Kingdom and New York, NY, USA

Clarke, L., Edmonds, J., Krey, V., Richels, R., Rose, S., & Tavoni, M. (2009). International Climate Policy architectures: Overview of the EMF 22 international scenarios. Energy Economics; International, U.S.and E.U. Climate Change Control Scenarios: Results from EMF 22, 31, Supplement 2, S64-S81. Retrieved from http://www.sciencedirect.com.proxy.lib.sfu.ca/science/article/pii/S0140988309001960

Claussen, M., Mysak, L., Weaver, A., Crucifix, M., Fichefet, T., Loutre, M., … Wang,Z. (2002). Earth system models of intermediate complexity: Closing the gap in the spectrum of climate system models. Climate Dynamics, 18(7), 579-586. doi: 10.1007/s00382-001-0200-1

Denman, K. L. (2008). Climate change, ocean processes and ocean iron fertilization. *Mar Ecol Prog Ser, 364*, 219-225. Retrieved from http://www.int-res.com.proxy.lib.sfu.ca/abstracts/meps/v364/p219-225/

Eby, M., Weaver, A. J., Alexander, K., Zickfeld, K., Abe-Ouchi, A., Cimatoribus, A. A., … Zhao, F. (2013). Historical and idealized climate model experiments: An intercomparison of earth system models of intermediate complexity. Climate of the Past, 9(3), 1111-1140. doi:10.5194/cp-9-1111-2013

Eby, M., Zickfeld, K., Montenegro, A., Archer, D., Meissner, K. J., & Weaver, A. J. (2009). Lifetime of anthropogenic climate change: Millennial time scales of potential CO_2 and surface temperature perturbations. Journal of Climate, 22(10), 2501-2511. doi: 10.1175/2008JCLI2554.1

Elzen, M. J., Vuuren, D., & Vliet, J. (2010). Postponing emission reductions from 2020 to 2030 increases climate risks and long-term costs. Climatic Change, 99, 313-320.

Ewen, T. L., Weaver, A. J., & Eby, M. (2004). Sensitivity of the inorganic ocean carbon cycle to future climate warming in the UVic coupled model. *Atmosphere-Ocean, 42*(1), 23-42. doi:10.3137/ao.420103

Flato, G., Marotzke, J., Abiodun, B., Braconnot, P., Chou, S.C., Collins, W.,… Rummukainen, M. (2013). Evaluation of Climate Models. In: Climate Change 2013: The Physical Science Basis. Contribution of Working Group I to the Fifth Assessment Report of the Intergovernmental Panel on Climate Change [Stocker, T.F., Qin, D., Plattner, G.-K., Tignor, M., Allen, S.K., Boschung, J.,… Midgley, P.M.]. Cambridge University Press, Cambridge,United Kingdom and New York, NY, USA

Frölicher, T., & Joos, F. (2010). Reversible and irreversible impacts of greenhouse gas emissions in multi-century projections with the NCAR global coupled carbon cycle-climate model. Climate Dynamics, 35(7-8), 1439-1459. doi: 10.1007/s00382-009-0727-0

Friedlingstein, P., Cox, P., Betts, R., Bopp, L., Von Bloh, W., Brovkin, V., … Fung, I. (2006). Climate-carbon cycle feedback analysis: Results from the C4MIP model intercomparison. J.Clim. 19: 3337-3353.

Gillett, N. P., Arora, V. K., Matthews, D., & Allen, M. R. (2013). Constraining the ratio of global warming to cumulative CO_2 emissions using CMIP5 simulations. Journal of Climate, 26(18), 6844-6858. doi:10.1175/JCLI-D-12-00476.1

Gillett, N. P., Arora, V. K., Zickfeld, K., Marshall, S. J., & Merryfield, W. J. (2011). Ongoing climate change following a complete cessation of carbon dioxide emissions. Nature Geosci, 4(2), 83-87. Retrieved from http://dx.doi.org.proxy.lib.sfu.ca/10.1038/ngeo1047

Hansen, J., Nazarenko, L., Ruedy, R., Sato, M., Willis, J., Del Genio, A., … Tausnev, N. (2005). Earth's energy imbalance: Confirmation and implications. Science, 308(5727), 1431-1435. Retrieved from http://www.sciencemag.org.proxy.lib.sfu.ca/content/308/5727/1431.abstract

Heimann, M., & Reichstein, M. (2008). Terrestrial ecosystem carbon dynamics and climate feedbacks. Nature, 451, 289-292.

Held, I. M., Winton, M., Takahashi, K., Delworth, T., Zeng, F., & Vallis, G. K. (2010). Probing the fast and slow components of global warming by returning abruptly to preindustrial forcing. Journal of Climate, 23(9), 2418-2427. doi: 10.1175/2009JCLI3466.1

IPCC (2007). Climate Change 2007: The Physical Science Basis. Contribution of Working Group I to the Fourth Assessment Report of the Intergovernmental Panel on Climate Change [Solomon, S., Qin, D., Manning, M., Chen, Z., Marquis, M., Averyt, K.B., … Miller, H.L.]. Cambridge University Press, Cambridge, United Kingdom and New York, NY, USA.

IPCC (2013). Climate Change 2013: The Physical Science Basis. Contribution of Working Group I to the Fifth Assessment Report of the Intergovernmental Panel on Climate Change [Stocker, T.F., Qin, D., Plattner, G.-K., Tignor, M., Allen, S.K., Boschung, J.,… Midgley, P.M.]. Cambridge University Press, Cambridge,United Kingdom and New York, NY, USA

Joos, F., Roth, R., Fuglestvedt, J. S., Peters, G. P., Enting, I. G., von Bloh, W., . . . Weaver, A. J. (2013). Carbon dioxide and climate impulse response functions for the computation of greenhouse gas metrics: A multi-model analysis. *Atmospheric Chemistry and Physics, 13*(5), 2793-2825. doi:10.5194/acp-13-2793-2013

Keith, D.W., Ha-Duong, M., & Stolaroff, J.K. (2006). Climate strategy with CO_2 capture from the air. Climatic change, 74 (1-3), 17-45. doi:10.1007/s10584-005-9026-x

Krey, V., & Riahi, K. (2009). Implications of delayed participation and technology failure for The feasibility, costs, and likelihood of staying below temperature targets: greenhouse gas mitigation scenarios for the 21st century. Energy Economics; International, U.S.and E.U.Climate Change Control Scenarios: Results from EMF 22, 31, Supplement 2(0), S94-S106. Retrieved from http://www.sciencedirect.com.proxy.lib.sfu.ca/science/article/pii/S0140988309001170

Kriegler, E., Edenhofer, O., Reuster, L., Luderer, G., & Klein, D. (2013). Is atmospheric carbon dioxide removal a game changer for climate change mitigation? Climatic Change, 118(1), 45-57. doi: 10.1007/s10584-012-0681-4

Kump, L. R., Kasting, J. F., & Crane, R. G. (2010). The Earth System. Pearson College Div.San Francisco: Prentice Hall

Kypreos, S. (2012). From the Copenhagen accord to efficient technology protocols. Energy Policy, 44(0), 341-353. doi: http://dx.doi.org.proxy.lib.sfu.ca/10.1016/j.enpol.2012.01.063

Lackner, K. S., Brennan, S., Matter, J. M., Park, A. A., Wright, A., & van der Zwaan, B.(2012). The urgency of the development of CO2 capture from ambient air. Proceedings of the National Academy of Sciences}, doi: 10.1073/pnas.1108765109

Lackner, K.S., Grimes, P., & Ziock, H.K., (2001). Capturing carbon dioxide from air. Proceedings of the First International Sequestration Conference (Department of Energy National Energy Technology Laboratory, Alexandria, VA), Session 7B:Capture, V: Adsorption Studies, 1–15.

Le Quere, C., Andres, R.J., Boden, T., Conway, T., Houghton, R., House, J.I., … Ahlström, A. (2013). The global carbon budget 1959-2011. Earth System Science Data 5: 165-185.

Le Quéré, C., Raupach, M. R., Canadell, J. G., & Marland, E. A. (2009). Trends in the sources and sinks of carbon dioxide. Nature Geosci, 2(12), 831-836. Retrieved from http://dx.doi.org.proxy.lib.sfu.ca/10.1038/ngeo689

Lowe, J.A., Huntingford, C., Raper, S.C.B., Jones, C.D., Liddicoat, S.K., & Gohar, L.K. (2009). How difficult is it to recover from dangerous levels of global warming? Environmental Research Letters, 4(1), 014012. Retrieved from http://stacks.iop.org.proxy.lib.sfu.ca/1748-9326/4/i=1/a=014012

MacDougall, A. H. (2013). Reversing climate warming by artificial atmospheric carbon-dioxide removal: Can a Holocene-like climate be restored? Geophysical Research Letters, 40, 5480-5485.

MacDougall, A.H., Avis, C.A., & Weaver, A.J. (2012). Significant contribution to climate warming from the permafrost carbon feedback. Nature Geoscience, 5, 719-721.

Macintosh, A. (2010). Keeping warming within the 2°C limit after Copenhagen. Energy Policy; the Role of Trust in Managing Uncertainties in the Transition to a Sustainable Energy Economy,Special Section with Regular Papers, 38(6), 2964-2975. doi: http://dx.doi.org.proxy.lib.sfu.ca/10.1016/j.enpol.2010.01.034

Matthews, H. D., & Caldeira, K. (2008). Stabilizing climate requires near-zero emissions. Geophysical Research Letters, 35(4), L04705. doi: 10.1029/2007GL032388

Matthews, H. D., Gillett, N. P., Stott, P. A., & Zickfeld, K. (2009). The proportionality of global warming to cumulative carbon emissions. Nature, 459(7248), 829-832. Retrieved from http://dx.doi.org.proxy.lib.sfu.ca/10.1038/nature08047

McGlashan, N., Shah, N., Caldecott, B., & Workman, M. (2012) High-level techno-economic assessment of negative emissions technologies. Process Safety and Environmental Protection. Retrieved from http://www.sciencedirect.com.proxy.lib.sfu.ca/science/article/pii/S0957582012001164

McGlashan N., Shah N., & Workman M. (2010). The Potential for the Deployment of Negative Emissions Technologies in the UK. Work stream 2, Report 18 of the AVOID programme (AV/WS2/D1/R18). Retrieved from: www.avoid.uk.net

McGuffie, K., & Henderson-Sellers, A. (2001). Forty years of numerical climate modelling. International Journal of Climatology, 21(9), 1067-1109. doi: 10.1002/joc.632

Meissner, K. J., Weaver, A. J., Matthews, H. D., & Cox, P. M. (2003). The role of land surface dynamics in glacial inception: A study with the UVic earth system model. Climate Dynamics, 21(7-8), 515-537. doi: 10.1007/s00382-003-0352-2

Orr, J.C., Najjar, R., Sabine, C.L., & Joos, F. (1999). Abiotic-HOWTO. Internal OCMIP Report, LSCE/CEA Saclay, Gif-sur-Yvette, France. 29 pp.

Plattner, G., Knutti, R., Joos, F., Stocker, T., Von Bloh, W., Brovkin, V., … Eby, M. (2008). Long-term climate commitments projected with climate-carbon cycle models. Journal of Climate, 21, 2721-2751.

Pond, S., & Pickard, G.L. (1995). *Introductory Dynamical Oceanography*. Oxford: Butterworth-Heinemann.

Ranjan, M., & Herzog, H. J. (2011). Feasibility of air capture. Energy Procedia; 10th International Conference on Greenhouse Gas Control Technologies, 4(0), 2869-2876. Retrieved from http://www.sciencedirect.com.proxy.lib.sfu.ca/science/article/pii/S1876610211003900

Rogelj, J., Hare, W., Lowe, J., van Vuuren, D. P., Riahi, K., Matthews, B., … Meinshausen, M. (2011). Emission pathways consistent with a 2°C global temperature limit. Nature Clim.Change,1(8), 413-418. Retrieved from http://dx.doi.org.proxy.lib.sfu.ca/10.1038/nclimate1258

Schmittner, A., Oschlies, A., Giraud, X., Eby, M., & Simmons, H. L. (2005). A global model of the marine ecosystem for long-term simulations: Sensitivity to ocean mixing, buoyancy forcing, particle sinking, and dissolved organic matter cycling. Global Biogeochemical Cycles, 19(3), n/a-n/a. doi: 10.1029/2004GB002283

Schmittner, A., Oschlies, A., Matthews, H. D., & Galbraith, E. D. (2008). Future changes in climate, ocean circulation, ecosystems, and biogeochemical cycling simulated for a business-as-usual CO2 emission scenario until year 4000 AD. Global Biogeochemical Cycles, 22(1), n/a-n/a. doi: 10.1029/2007GB002953

Solomon, S., Plattner, G. K., Knutti, R., & Friedlingstein, P. (2009). Irreversible climate change due to carbon dioxide emissions Proceedings of the National Academy of Sciences of the United States of America, 106(6), 1704-1709. doi: 10.1073/pnas.0812721106

Tavoni, M. & Socolow, R. (2013). Modeling meets science and technology: an introduction to a special issue on negative emissions. Climatic Change, 118, 1-14.

UNFCCC (2009). Conference of the Parties. Report of the Conference of the Parties on its fifteenth session, held in Copenhagen from 7 to 19 December 2009. Addendum. Part Two: Action taken by the Conference of the Parties at its fifteenth session. Retrieved 11/20/2012, 2012, from http://unfccc.int/documentation/documents/advanced_search/items/6911.php?prir ef=600005735#beg

UNFCCC (1992). The United Nations Framework Convention on Climate Change – Article II. Retrieved 11/20/2012, 2012, from http://unfccc.int/essential_background/convention/background/items/1353.php

Vichi, M., Navarra, A., & Fogli, P.G. (2013). Adjustment of the natural ocean carbon cycle to negative emission rates. Clim. Change 118, 105-118.

Vuuren, D. P., Elzen, M.G.J., Lucas, P., Eickhout, B., Strengers, B.J., Ruijven, B., … Houdt, R. (2007). Stabilizing greenhouse gas concentrations at low levels: an assessment of reduction strategies and costs. Clim. Change 81, 119-159.

Weaver, A. J., Eby, M., Wiebe, E. C., Bitz, C. M., Duffy, P. B., Ewen, T. L., … Yoshimori, M. (2001). The UVic earth system climate model: Model description, climatology, and applications to past, present and future climates. Atmosphere Ocean, 39(4), 361-428.

Weaver, A. J., Zickfeld, K., Montenegro, A., & Eby, M. (2007). Long term climate implications of 2050 emission reduction targets. Geophysical Research Letters, 34(19), n/a-n/a. doi: 10.1029/2007GL031018

Wild, M., Folini, D., Schär, C., Loeb, N., Dutton, E., & König-Langlo, G. (2013). The global energy balance from a surface perspective. Climate Dynamics, 40(11-12), 3107-3134. doi:10.1007/s00382-012-1569-8

Workman, M., McGlashan, N., Chalmers, H., & Shah, N. (2011). An assessment of options for CO2 removal from the atmosphere. Energy Procedia; 10th International Conference on Greenhouse Gas Control Technologies, 4(0), 2877-2884. Retrieved from http://www.sciencedirect.com.proxy.lib.sfu.ca/science/article/pii/S1876610211003912

Zickfeld, K., Arora, V. K., & Gillett, N. P. (2012). Is the climate response to CO_2 emissions path dependent? Geophysical Research Letters, 39(5), L05703. doi: 10.1029/2011GL050205

Zickfeld, K., Eby, M., Alexander, K., Weaver, A. J., Crespin, E., Fichefet, T., … Zhao, P. (2013). Long term climate change commitment and reversibility: An EMIC intercomparison. Journal of Climate, 26, 5782–5809. doi: 10.1175/JCLI-D-12-00584.1

Zickfeld, K., Eby, M., Matthews, H. D., Schmittner, A., & Weaver, A.J. (2011). Nonlinearity of carbon cycle feedbacks. Journal of Climate, 24, 4255–4275. doi: http://dx.doi.org/10.1175/2011JCLI3898.1

Zickfeld, K., Eby, M., Matthews, H. D., & Weaver, A. J. (2009). Setting cumulative emissions targets to reduce the risk of dangerous climate change. Proceedings of the National Academy of Sciences, 106(38), 16129-16134. doi: 10.1073/pnas.0805800106